

High-Energy Neutrinos Produced by Interactions of Relativistic Protons in Shocked Pulsar Winds

Shigehiro Nagataki^{1,2}

¹*Department of Physics, School of Science, University of Tokyo,
7-3-1 Hongo, Bunkyo, Tokyo 113-0033, Japan*

²*Research Center for the Early Universe, School of Science, University of Tokyo,
7-3-1 Hongo, Bunkyo, Tokyo 113-0033, Japan*

nagataki@utap.phys.s.u-tokyo.ac.jp

ABSTRACT

We have estimated fluxes of neutrinos and gamma-rays that are generated from decays of charged and neutral pions from a pulsar surrounded by supernova ejecta in our galaxy, including an effect that has not been taken into consideration, that is, interactions between high energy cosmic rays themselves in the nebula flow, assuming that hadronic components are the energetically dominant species in the pulsar wind. Bulk flow is assumed to be randomized by passing through the termination shock and energy distribution functions of protons and electrons behind the termination shock are assumed to obey the relativistic Maxwellians. We have found that fluxes of neutrinos and gamma-rays depend very sensitively on the wind luminosity, which is assumed to be comparable to the spin-down luminosity. In the case where $B = 10^{12}\text{G}$ and $P = 1\text{ms}$, neutrinos should be detected by km^3 high-energy neutrino detectors such as AMANDA and IceCube. Also, gamma-rays should be detected by Cherenkov telescopes such as CANGAROO and H.E.S.S. as well as by gamma-ray satellites such as GLAST. On the other hand, in the case where $B = 10^{12}\text{G}$ and $P = 5\text{ms}$, fluxes of neutrinos and gamma-rays will be too low to be detected even by the next-generation detectors. However, even in the case where $B = 10^{12}\text{G}$ and $P = 5\text{ms}$, there is a possibility that very high fluxes of neutrinos may be realized at early stage of a supernova explosion ($t \leq 1\text{yr}$), where the location of the termination shock is very near to the pulsar. We also found that there is a possibility that protons with energies $\sim 10^5\text{ GeV}$ in the nebula flow may interact with the photon field from surface of the pulsar and produce much pions, which enhances the intensity of resulting neutrinos and gamma-rays.

Subject headings: acceleration of particles — neutrinos — shock waves — pulsars:
general — stars: winds, outflows — gamma-rays

1. Introduction

It has been about 35 years since Goldreich and Julian (1969) pointed out that a rotating magnetic neutron star generates huge electric potential differences between different parts of its surface and, as a result, should be surrounded with charged plasma, which is called a magnetosphere. Gunn and Ostriker (1969) also pointed out the possibility that a rotating magnetic neutron star may be a source of high energy cosmic rays. Such high energy cosmic rays are considered to be driven along magnetic field lines since these lines do not cross. Also, since part of the magnetic fields around the neutron star passes through the light cylinder, which means such magnetic fields are open, accelerated charged particles are driven to outside of the light cylinder, which are called as pulsar winds. The pulsar winds are usually considered to be composed of electron-positron pairs since electron-positron pairs will be created so as to eliminate electric fields that are parallel to magnetic fields at a region where net charge density is not equal to the Goldreich-Julian density (Ruderman and Sutherland 1975; Shibata 1991). However, it is also pointed out that hadronic component may exist in pulsar winds as a consequence of the net charge neutrality in the outflow (Hoshino et al. 1992; Bednarek and Protheroe 1997; Protheroe et al. 1998; Blasi et al. 2000; Amato et al. 2003). Moreover, it is pointed out that hadronic components may be the energetically dominant species although they are dominated by electron-positron pairs in number (Hoshino et al. 1992). This is because inertial masses of hadrons are much larger than that of electron.

Based on the assumption that hadronic components are not negligible in pulsar winds, some scenarios are proposed to produce high energy neutrinos and gamma-rays from decays of charged and neutral pions that are produced by interactions between hadronic, accelerated high energy cosmic rays and surrounding photon fields and/or matter. Atoyan and Aharonian (1996) estimated flux of gamma-rays and discussed its contribution on the observed spectrum of the Crab nebula, although they concluded that its contribution may be important only at energies above 10 TeV. Bednarek and Protheroe (1997) proposed that accelerated heavy nuclei can be photo-disintegrated in the pulsar's outer gap, injecting energetic neutrons which decay into protons. The protons from neutron decay inside the supernova ejecta should accumulate, producing neutrinos and gamma-rays in collisions with the matter

in the supernova ejecta.¹ There are some papers based on this scenario and flux of neutrinos and/or gamma-rays is estimated (Protheroe et al. 1998; Bednarek and Bartosik 2003; Bednarek 2003a; Bednarek 2003b; Amato et al. 2003). Beal and Bednarek (2002) proposed that accelerated cosmic rays will interact with the photon fields inside the supernova remnant at the very early phase (within ~ 1 yr) of a supernova explosion. Bednarek (2001) calculated the extragalactic neutrino background based on this scenario.

In this study, we estimate fluxes of neutrinos and gamma-rays including an effect that has not been taken into consideration, that is, interactions between high energy cosmic rays themselves. This picture is based on the works given by Rees and Gunn (1974) and Kennel and Coroniti (1984). Rees and Gunn (1974) pointed out that the supersonic pulsar wind would terminate in a standing reverse shock located at a distance r_s from the pulsar. Beyond the termination shock, the highly relativistic, supersonic flow is randomized and bulk speed becomes subsonic, obeying the Rankine-Hugoniot relations. According to Hoshino et al. (1992), who studied the theoretical properties of relativistic, transverse, magnetosonic collisionless shock waves in electron-positron-heavy ion plasmas, proton distribution functions in the down stream are found to be almost exactly described by relativistic Maxwellians with temperatures $T_{p,2}/\gamma_1 m_p c^2 \sim 0.34$, where $T_{p,2}$ is temperature at the down stream, γ_1 is the bulk Lorentz factor of protons in the up stream. It is noted that protons are not thermalized through the interactions with protons themselves, and/or electrons but just obeys the Maxwellian distribution through transferring cyclotron waves. This subsonic flow speed would be, by communicating with the nebula boundary at r_N via sound waves, adjusted to match the expansion speed of the supernova remnant (that is, supernova ejecta) at the innermost region. This subsonic flow is called as nebula flow in the study of Kennel and Coroniti (1984). We also adopt this definition in this study. In this study, we calculate flux of neutrinos and gamma-rays from charged and neutral pion decays in the nebula flow which are produced through the interactions between high energy protons themselves, assuming that energy distribution functions of protons obey the relativistic Maxwellians.

In this study, as the previous works, we assume that protons are energetically dominant in the pulsar winds. Thus, we describe the nebula flow using the proton mass as a unit of mass. We estimate pion production rates due to the interactions between high energy protons using proper Lorentz transformations. As for the cross sections between protons, scaling model (Badhwar et al. 1977) is adopted. Isobar model is not included in this study since we consider production rates of high energy pions. Calculating the spectrum of neutrinos

¹They call this region as a nebula, which is slightly different from the definition of a nebula given by Kennel and Coroniti (1984). In this study, as explained below, we adopt the definition presented by Kennel and Coroniti (1984).

and gamma-rays in the termination shock rest frame, we estimate these fluxes at the earth assuming that the pulsar is located at 10 kpc away from the earth.

In section 2, we explain the formulation in this study. Results are shown in section 3. Discussions are given in section 4. Summary and conclusion are presented in section 5.

2. FORMULATION

2.1. Confinement of Pulsar Wind by the Surrounding Supernova Remnant

In this subsection, we briefly review the steady state, spherically symmetric, magnetohydrodynamic model of nebula flow presented by Kennel and Coroniti (1984), in which a highly relativistic pulsar wind is terminated by a strong MHD shock that decelerates the flow and increases its pressure to match the boundary conditions imposed by the surrounding supernova remnant. In this study, we consider the possibility that the protons are the energetically dominant species in the flow as pointed by Hoshino et al. (1992). According to the work presented by Hoshino et al. (1992), the proton distribution functions behind the termination shock are almost exactly described by relativistic Maxwellians. Thus we can define temperature behind the shock wave and solve the following nebula flow using the magnetohydrodynamic equations.

2.1.1. Super-relativistic Magnetohydrodynamic Shock

It is usually introduced the parameter σ , which is the ratio of the magnetic plus electric flux to the particle energy flux at just ahead of the termination shock,

$$\sigma = \frac{B^2}{4\pi n u \Gamma m_p c^2}, \quad (1)$$

where B is the amplitude of the magnetic field in the observer's frame, n is the proper density, u is the radial four speed of the flow, Γ is the bulk Lorentz factor of the flow ($\Gamma^2 = 1 + u^2$), m_p is the proton mass, c is the speed of light. It is assumed that the energy density of electric field is nearly equal to that of magnetic field. The luminosity L at just ahead of the termination shock is described as

$$L = 4\pi n \Gamma u r_s^2 m_p c^3 (1 + \sigma), \quad (2)$$

where r_s is the radius of the termination shock. The termination shock is assumed to be stationary relative to the pulsar and the observer. Thus the Rankine-Hugoniot relations

for 90° shocks can be used directly to obtain the physical quantum in the observer’s frame behind the shock wave:

$$n_1 u_1 = n_2 u_2 \quad (3)$$

$$E = \frac{u_1 B_1}{\Gamma_1} = \frac{u_2 B_2}{\Gamma_2} \quad (4)$$

$$\Gamma_1 \mu_1 + \frac{E B_1}{4\pi n_1 u_1} = \Gamma_2 \mu_2 + \frac{E B_2}{4\pi n_2 u_2} \quad (5)$$

$$\mu_1 u_1 + \frac{P_1}{n_1 u_1} + \frac{B_1^2}{8\pi n_1 u_1} = \mu_2 u_2 + \frac{P_2}{n_2 u_2} + \frac{B_2^2}{8\pi n_2 u_2}. \quad (6)$$

Subscripts 1 and 2 label upstream and downstream parameters. E denotes the shock frame electric fields and $\mu = (e + P)/n$ is the specific enthalpy, which for a gas with an adiabatic index γ is defined by

$$\mu = mc^2 + \frac{\gamma}{\gamma - 1} \left(\frac{P}{n} \right). \quad (7)$$

In this study, we set γ_2 to be 4/3, as explained in Appendix A.

Kennel and Coroniti (1984) introduced a parameter Y to obtain the downstream radial four speed, u_2 . Definition of Y is

$$Y \equiv \frac{B_2}{B_1} = \frac{\Gamma_2 u_1}{\Gamma_1 u_2}. \quad (8)$$

Using this parameter and $\gamma_2 = 4/3$, Eq. (6) can be expressed as

$$Y^2 - Y \left[\frac{2}{\Gamma_2 u_2} \left(u_2^2 + \frac{1}{4} \right) \frac{u_1}{\Gamma_1} \right] + \left[\frac{2}{\Gamma_2 u_2} \left(u_2^2 + \frac{1}{4} \right) \left(\frac{4\pi n_1 \mu_1 \Gamma_1^2 u_1}{B_1^2 \Gamma_1} \right) \right] - \frac{2\pi n_1 m_p c^2 u_1}{B_1^2 u_2} - \left(1 + \frac{8\pi(n_1 \mu_1 u_1^2 + P_1)}{B_1^2} \right) = 0. \quad (9)$$

Although there are some trivial typos for the expression of Eq. (9) in the original paper, they does not affect the following discussion.

Assuming that the bulk Lorentz factor of the pulsar wind is sufficiently large and the flow is sufficiently cold, we can approximate Γ_1 , P_1 , and μ_1 as $\Gamma_1 \sim u_1$, $P_1 \sim 0$, and $\mu_1 \sim m_p c^2$. Using these approximations, we can rewrite Eq. (9) as

$$u_2^2 \left(u_2^2 + \frac{1}{4} \right)^2 = (1 + u_2^2) \left(u_2^2 - \frac{1}{4} \frac{\sigma}{1 + \sigma} \right)^2. \quad (10)$$

Solving Eq. (10), we can obtain the radial four speed behind the shock wave as

$$u_2^2 = \frac{8\sigma^2 + 10\sigma + 1}{16(\sigma + 1)} + \frac{1}{16(\sigma + 1)} [64\sigma^2(\sigma + 1)^2 + 20\sigma(\sigma + 1) + 1]^{1/2}. \quad (11)$$

Note that the radial four velocity behind the shock wave is determined by only one parameter, σ .

As for the pressure P_2 , it can be obtained as

$$\frac{P_2}{n_1 m_p c^2 u_1^2} = \frac{1}{4u_2 \Gamma_2} \left[1 + \sigma \left(1 - \frac{\Gamma_2}{u_2} \right) \right], \quad (12)$$

where we assumed that $\mu_2 \sim 4(P_2/n_2)$.

In this study, we adopt a slightly different way to determine the temperature from the way presented by Kennel and Coroniti (1984), using the results of Hoshino et al. (1992). According to Hoshino et al. (1992), the distribution functions of protons behind the termination shock are almost exactly described by relativistic Maxwellians as

$$N(\gamma) = A\gamma \exp \left[-\frac{m_p c^2}{k_B T} (\gamma - 1) \right], \quad (13)$$

where γ is the Lorenz factor that represents the random motion (note that this is not the adiabatic index), k_B is the Boltzmann constant and A is the normalization factor in units of cm^{-3} . In this case, the relation

$$P_2 = \frac{2}{3} n_2 k_B T_2 \quad (14)$$

holds exactly (see Appendix A in detail). Thus the temperature T_2 can be derived from Eqs. (12) and (14) as

$$\frac{k_B T_2}{u_1 m_p c^2} = \frac{3}{8\Gamma_2} \left[1 + \sigma \left(1 - \frac{\Gamma_2}{u_2} \right) \right]. \quad (15)$$

As a result, we can estimate the energy density (e) [erg cm^{-3}] as

$$e = A m_p c^2 e^\alpha \int_1^\infty \gamma^2 e^{-\alpha\gamma} d\gamma, \quad (16)$$

where $\alpha = m_p c^2 / k_B T$. Since we can obtain the physical quantum just behind the termination shock, we consider the resulting flow from the termination shock to the remnant. This flow is usually called as nebula flow.

2.1.2. Nebula Flow

The steady and spherically symmetric nebula flow is described by the equations mentioned below. These are; the equation describing the conservation of number flux,

$$\frac{d}{dr}(cnur^2) = 0; \quad (17)$$

one describing the conservation of magnetic flux in the magnetohydrodynamic approximation,

$$\frac{d}{dr} \left(\frac{ruB}{\Gamma} \right) = 0; \quad (18)$$

one describing the propagation of thermal energy,

$$\frac{d}{dr} (ur^2e) + P \frac{d}{dr} (r^2u) = 0; \quad (19)$$

and one describing the conservation of total energy,

$$\frac{d}{dr} \left[nur^2 \left(\Gamma\mu + \frac{B^2}{4\pi n\Gamma} \right) \right] = 0. \quad (20)$$

Note that the notation for the thermal energy density is slightly different from the original paper.

When the relation $e = 3P$ holds, Eq.(19) reduces to

$$\frac{d}{dr} \ln \left(\frac{P}{n^{4/3}} \right) = 0. \quad (21)$$

These are the basic equations describing the nebula flow which connects the condition behind the termination shock and the inner-edge of the supernova remnant.

Here we assumed that the distribution functions of protons remain Maxwellian and temperature can be determined at each radius of the nebula flow. However, we should adopt the Boltzmann equations coupled with the evolution of magnetic fields to obtain the exact solution for the nebula flow, since it is not apparent for protons to transfer their energies with each other enough to obey the Maxwellian distribution. However, as shown in section 3, charged and neutral pions are mainly produced just behind the termination shock (see also figures 8 and 12), where the energy distribution of protons obey relativistic Maxwellian. The nebula flow can be described approximately as a free-expansion and temperature and density in the nebula flow becomes smaller along with radius, which means pions are less produced along with radius. Thus we consider that the order-estimate of the neutrino flux produced

by pp collisions will be valid even if the MHD equations are adopted. We will estimate the neutrino flux using the Boltzmann equations coupled with the evolution of magnetic fields in the forthcoming paper.

The solution for the nebula flow can be obtained analytically (see Appendix C for details). Using the solution, total pressure P_T in the postshock can be expressed as

$$P_T = P + \frac{E^2 + B^2}{8\pi} = \frac{L}{4\pi r_s^2 c(1 + \sigma)} \left[\frac{P_2}{n_1 m_p c^2 u_1^2} (vz^2)^{-4/3} + \frac{\sigma}{z^2} \left(1 + \frac{1}{2u_2^2 v^2} \right) \right], \quad (22)$$

where v is defined as $v = u/u_2$ and z is defined as $z = r/r_s$.

As explained in section 2.1.3, we investigate the case $\sigma \ll 1$, because the speed of the nebula flow at the boundary between the remnant and nebula flow is set to be almost same with the speed of the remnant ($\sim 2000 \text{ km s}^{-1}$). In the case of $\sigma \ll 1$,

$$u_2 \sim \left(\frac{1 + 9\sigma}{8} \right)^{1/2} \quad (23)$$

and

$$\frac{P_2}{n_1 m_p c^2 u_1^2} \sim \frac{2}{3} (1 - 7\sigma). \quad (24)$$

Thus the total pressure can be written approximately

$$P_T \sim \frac{2}{3} (n_1 \Gamma_1 u_1 m_p c^2) \left[\frac{1 - 7\sigma}{(vz^2)^{4/3}} + \frac{\sigma}{z^2} \left(1 + \frac{4}{v^2} \right) \right]. \quad (25)$$

This approximation is used in section 2.1.3.

2.1.3. Boundary Conditions

As for the inner boundary condition, the parameters are bulk Lorentz factor and luminosity of the wind. As for the bulk Lorentz factor, we can estimate its upper limit as a function of the rotation period and the amplitude of the polar magnetic field of the pulsar (Goldreich and Julian 1969). The corotating magnetosphere is bounded by a field line whose feet are at $\sin \theta_o \sim (\Omega R/c)^{1/2} = (2R/P)^{1/2} \times 10^{-5}$, where θ_o is the zenith angle (in a unit of rad), Ω is the angular velocity of the pulsar, R is the radius (in a unit of cm), and P is the rotation period (in a unit of s). The potential difference between θ_o and the pole is

$$\Delta\Phi = \frac{1}{2} \left(\frac{\Omega R}{c} \right)^2 R B_p \quad (26)$$

for $\Omega R/c \ll 1$ when the surrounding region of the pulsar is vacuum. Here B_p is the amplitude of the polar magnetic field in units of G. Although the magnetosphere should be filled with plasma whose number density is the Goldreich-Julian value, the most energetic escaping particles can be estimated using Eq. (26). It will be $\sim \Delta\Phi/2$, or

$$\epsilon_{\max} = 3 \times 10^{18} Z \left(\frac{B_p}{10^{12}\text{G}} \right) \left(\frac{1\text{ms}}{P} \right)^2 \left(\frac{R}{10^6\text{cm}} \right)^3 \text{ eV}, \quad (27)$$

where Z is the atomic charge. Thus the bulk Lorentz factor of protons can be estimated as

$$\Gamma_{\max} = 3.2 \times 10^9 \left(\frac{B_p}{10^{12}\text{G}} \right) \left(\frac{1\text{ms}}{P} \right)^2 \left(\frac{R}{10^6\text{cm}} \right)^3. \quad (28)$$

In this study, we assume that the bulk Lorentz factor of the pulsar wind is monolithic and its upper limit is given by Eq. (28).

The wind luminosity can be estimated when it is assumed to be comparable to the pulsar's spin down luminosity. Under the assumption, it can be expressed as

$$L = 9.6 \times 10^{42} \left(\frac{B_p}{10^{12}\text{G}} \right)^2 \left(\frac{R}{10^6\text{cm}} \right)^6 \left(\frac{1\text{ms}}{P} \right)^4 \text{ erg s}^{-1}. \quad (29)$$

In this case, the angular velocity evolves as a function of time as

$$\Omega(t) = \Omega_i \left(1 + \frac{B^2 R^6 \Omega_i^2}{3c^3 I} t \right)^{-1/2} \text{ rad s}^{-1}, \quad (30)$$

where Ω_i and $I \sim 10^{45} \text{ g cm}^2$ are initial angular velocity and inertial moment of a pulsar, respectively. We can estimate the spindown age which is defined as the time when the angular velocity $\Omega(t)$ becomes $2\Omega_i$ as

$$t_{\text{spin}} \equiv 6.2 \times 10^9 \left(\frac{10^{12}\text{G}}{B_p} \right)^2 \left(\frac{10^6\text{cm}}{R} \right)^6 \left(\frac{P}{1\text{ms}} \right)^2 \text{ s}. \quad (31)$$

In figure 1, we show the spin down age [yr] as a function of period of a pulsar (solid line) as well as the spin down luminosity (dashed line). Amplitude of the magnetic field at the pole of a pulsar is set to be 10^{12}G in this study.

Next, we consider the outer boundary condition. It is naturally considered that the inner region of a supernova remnant is composed of He layer that includes heavy nuclei (Hashimoto 1995; Woosley and Weaver 1995; Thielemann et al. 1996; Nagataki et al. 1997; Nagataki 2000) whose escape velocity is $\sim 2000 \text{ km s}^{-1}$ for the free-expansion phase (Haas et al. 1990; Spyromilio et al. 1990). In this phase, the initial explosion energy is almost all manifested

by kinetic energy of the ejected matter; thermal energy comes to 2 or 3% of the initial explosion energy. Thus we model the innermost region of the ejecta as follows. We consider the $6M_{\odot}$ He layer which is the typical mass of helium for the progenitor of collapse-driven supernova (Hashimoto 1995). Then, the speed of the escaping velocities of the He layer is 2000 km s^{-1} ($=V_{\min}$) for the inner edge and 3000 km s^{-1} ($=V_{\max}$) for the outer edge. The thermal energy in the He layer is assumed to be

$$\begin{aligned} E_{\text{th}} &= 0.02 \times 10^{51} \times \frac{6M_{\odot}}{20M_{\odot}} \text{ erg} \\ &= 6 \times 10^{48} \text{ erg}, \end{aligned} \quad (32)$$

where 0.02 represents the fraction of the thermal energy in the ejecta, 10^{51} is the typical explosion energy of a collapse-driven supernova, $6M_{\odot}$ is the mass of the He layer and $20M_{\odot}$ is the typical total mass of the ejecta. Thus the volume occupied by the He layer can be calculated as

$$V = \frac{4}{3}\pi [V_{\max}^3 - V_{\min}^3] \left(\frac{t}{1\text{sec}}\right)^3, \quad (33)$$

where t is the age of the supernova remnant. Thus the typical pressure in the He layer can be estimated by solving the equations

$$E_{\text{th}} = \frac{3}{2}(N_e + N_{\text{He}})k_B T + 3aT^4 V \quad (34)$$

and

$$P = (n_e + n_{\text{He}})k_B T + aT^4, \quad (35)$$

where N_e and N_{He} are the total number of electron and helium in the He layer, n_e and n_{He} are the number density of electron and helium, and a is the radiation constant, respectively. Here we approximated that the He layer is composed of helium, neglecting the contamination of heavy nuclei. Using this model, we can estimate the pressure at the innermost region as a function of time and the result is shown in figure 2. The discontinuity at $t \sim 5 \text{ yr}$ reflects the transition from photon-dominated phase to matter-dominated phase. This happens when the optical depth of the supernova ejecta becomes lower than unity and pressure of photon fields is set to be zero.

As for the Crab nebula (age of the Crab is $\sim 1000\text{yr}$), the pressure at the innermost region of the remnant is estimated to be in the range $(1-10) \times 10^9 \text{ dyn cm}^{-2}$ (Kennel and Coroniti 1984). On the other hand, Iwamoto et al. (1997) estimated the pressure of the innermost region of the ejecta numerically and reported that $P \sim 10^{16} \text{ dyn cm}^{-2}$ at $t = 100 \text{ sec}$ ($\sim 3 \times 10^{-6}\text{yr}$).

We can find from figure 2 that the estimation by Eq. (35) reproduces these values fairly well. Thus we adopt this formula in this paper throughout.

Finally, we consider how to determine the position of the termination shock. The termination shock should be initiated at the innermost region of the remnant where the relativistic pulsar wind hits. Then, if the stationary state exists, the position of the termination shock propagates inward so as to attain the pressure balance between the nebula flow and remnant. If the pressure of the nebular flow (P_n) can not be comparable to that of the remnant (P_R), what happens? If (a) $P_n > P_R$, the nebula flow should push the remnant until the pressure balance is attained. In such a situation, interactions between relativistic protons in nebula flow and non-relativistic protons in the ambient remnant should be effective and may result in effective production of high energy neutrinos. This situation will be similar to that of the previous works such as Bednarek and Protheroe (1997). In such a situation, the interactions between the relativistic protons in the nebula flow and photons in the remnant may also become important, which will be similar to the situation that Beall and Bednarek (2002) presented. Such a situation is outscope of this study and detailed estimation of flux of high-energy neutrinos has been done by the previous works. On the other hand, if (b) $P_n < P_R$, the reverse shock initiated at the inner edge of the remnant would be driven back to the pulsar, as pointed out by Kennel and Coroniti (1984). This situation is within our scope and considered. These situations can be distinguished by using Eq. (25). The total pressure normalized by $2(n_1\Gamma_1u_1m_p c^2)/3 \sim P_2$ can be solved as a monotonic function of z , as shown in figure 3. In this figure, σ is set to be $6.7 \times 10^{-3} \equiv \sigma_c$, which is used throughout this paper as mentioned below. From the definition, $z_{\min} = 1$ and $z_{\max} = (R_{\text{rem}}/r_s)$, where $R_{\text{rem}} = 2 \times 10^8 t$ is the radius of the inner edge of the remnant at time = t sec. If the pressure in the remnant (P_R) is in the range $P_T(z = z_{\max}) \leq P_R \leq P_T(z = z_{\min})$, the radius of the termination shock is determined at r_s ($R \leq r_s \leq R_{\text{rem}}$). Otherwise, the situation is (a) $P_n > P_R$ or (b) $P_n < P_R$.

As for the velocity, the radial four velocity behind the shock wave depends on only one parameter, σ (Eq. (11)). Also, in the small σ limit, the asymptotic solution for $u_{r \rightarrow \infty}$ can be written as

$$u_\infty = \left(\frac{\sigma^2}{1 + 2\sigma} \right)^{1/2}, \quad (36)$$

which corresponds to

$$\beta_\infty = \frac{\sigma}{1 + \sigma}. \quad (37)$$

Thus σ should be $\sim 6.67 \times 10^{-3}$ in order to obtain the stationary nebula flow in which the velocity of the nebula flow is almost same with that of the innermost region of the remnant. In this study, we set $\sigma = \sigma_c$ throughout in this study for simplicity.

Of course, it is noted that the value of σ should be not determined by the outer boundary condition, but by pulsar's condition in principle. Thus our requirement, which is also adopted in Kennel and Coroniti (1984), may not be so realistic. Thus, before we go further, we should discuss here what will happen if (i) $\sigma > \sigma_c$ or (ii) $\sigma < \sigma_c$. In the case of (i), the speed of the nebula flow is faster than that of the remnant and additional pressure (ram pressure) is given to the nebula flow. Thus discussion on the pressure balance mentioned above should be modified by introducing the effect of the ram pressure when the ram pressure is comparable with or higher than the total pressure. In the case of (ii), as long as the contact discontinuity is adopted as a boundary condition, the location of the shock can not be far away from the remnant so that the nebula flow can catch up with the remnant. In this case, the resulting neutrino flux in the nebula flow should be small because the volume of the cavity (i.e. region between the shock and remnant) should be kept small. Also, there is a possibility that shocked region and remnant continue to separate from each other. If so, the rarefaction wave will be generated from the remnant and the rarefaction wave will connect the remnant and shocked region, achieving the boundary condition of contact discontinuity between rarefaction wave and shocked region. It will be important to investigate what kind of boundary condition is the most proper as a next step of this study.

2.2. Microphysics of Proton-Proton Interaction

In this section, the formulation of production of neutrinos and gamma-rays from pp collisions is presented. In section 2.2.1, we calculate at first the pion spectrum in the rest frame of the nebula flow. Then, the spectrum is transferred to the observer's frame. In section 2.2.2, microphysics of pp interactions is explained. Finally, we calculate the flux of neutrinos and gamma-rays as products of pion decays in section 2.2.3.

2.2.1. Formulation of Pion Production

First, we consider the number spectrum [particles $\text{cm}^{-3} \text{s}^{-1} \text{erg}^{-1}$] of charged and neutral pions in the rest frame of the nebula flow. It is calculated by considering two protons with four momenta p_1 and p_2 , moving towards each other with relative velocity v_{rel} . The number of collisions that occur in a volume dV , for a time dt , is a frame invariant quantity, which in an arbitrary reference frame can be written as (Landau and Lifshitz 1975; Mahadevan et al. 1997)

$$dR_{12} = \sigma_{pp} v_{\text{rel}} \frac{cp_1}{E_1} \frac{cp_2}{E_2} n_1 n_2 dV dt$$

$$= c\sigma_{pp}n_1n_2\sqrt{(\vec{\beta}_1 - \vec{\beta}_2)^2 - (\vec{\beta}_1 \times \vec{\beta}_2)^2}dVdt, \quad (38)$$

where σ_{pp} is the total cross section, n_1 and n_2 are the number density of protons with their four momenta are p_1 and p_2 , respectively. Thus the number spectrum of pions [particles $\text{cm}^{-3} \text{s}^{-1} \text{erg}^{-1}$] is calculated as

$$\begin{aligned} \frac{F(E_\pi)}{dV} &= c \int_1^\infty d\gamma_2 \int_1^{\gamma_2} d\gamma_1 \int_{-1}^1 d\cos\theta \frac{d\sigma_{pp}(\gamma_1, \gamma_2, \cos\theta)}{dE_\pi} n(R, \gamma_1)n(R, \gamma_2) \\ &\times \sqrt{(\vec{\beta}_1 - \vec{\beta}_2)^2 - (\vec{\beta}_1 \times \vec{\beta}_2)^2}, \end{aligned} \quad (39)$$

where γ_1, γ_2 are the respective Lorenz factors of the two protons, $\cos\theta = \vec{\beta}_1 \cdot \vec{\beta}_2 / |\vec{\beta}_1| |\vec{\beta}_2|$, R is the radius with respect to the neutron star, $n(R, \gamma)$ is the differential number density of protons at position R , and $d\sigma_{pp}(\gamma_1, \gamma_2, \cos\theta)/dE_\pi$ is the differential cross section of proton-proton interaction, which is explained in section 2.2.2. It is noted that the more energetic proton is labeled as 2 and the less energetic one is labeled as 1 in this formulation, which means γ_2 is always larger than γ_1 . In this frame, the distribution of pions in momentum space is isotropic. Thus the number spectrum of pions in unit solid angle [particles $\text{s}^{-1} \text{erg}^{-1} \text{sr}^{-1}$] is simply expressed as

$$\frac{dF(E_\pi)}{d\Omega} = \frac{1}{4\pi} \int_{\Delta V} \frac{F(E_\pi)}{dV} dV, \quad (40)$$

where Δ_V is the fluid element.

Next, we transfer the obtained number spectrum in the fluid-rest frame to the one in the observer's frame. It is noted that we consider a receiver in the observer's frame. Thus we consider both special relativistic effect and Doppler effect. The relative four velocity between the nebula flow and observer is considered to be $u(r)$ (i.e. we neglect the effect of proper motion of the pulsar with respect to the earth). The result is expressed as (see Appendix B for derivation)

$$\frac{d\bar{F}(\bar{E}_\pi)}{d\bar{\Omega}} = \frac{1}{\bar{\Gamma}^2(1 - \bar{\beta} \cos\bar{\theta})^2} \frac{F(E_\pi)}{4\pi}, \quad (41)$$

where bars are labeled for the quantum in observer's frame, $\bar{\theta}$ is the angle between the three dimensional velocity of the fluid element and direction of the observer measured from the fluid element, and $\bar{\Gamma}$ is the bulk Lorenz factor of the fluid element in the observer's frame. The relation between \bar{E}_π and E_π is expressed as

$$\bar{E}_\pi = \frac{1}{\bar{\Gamma}(1 - \bar{\beta} \cos\bar{\theta})} E_\pi. \quad (42)$$

This formulation is also used to calculate the flux of neutrinos and gamma-rays in the observer’s frame. In this study, however, this transformation is not so effective except for the region just behind the termination shock, because the speed of the flow behind the shock is not so high in the case of $\sigma \ll 1$ (see Eqs. (23) and (36)).

2.2.2. Differential Cross Section of Proton-Proton Interaction

We show the method of calculating the differential cross section of proton-proton interaction, $d\sigma_{pp}(\gamma_1, \gamma_2, \cos\theta)/dE_\pi$, which is introduced in section 2.2.1. We estimate this quantum by two steps. First, we transform the fluid-rest frame to the rest frame of particle 1 (i.e. laboratory frame), because formulation of the differential cross section for pion production in this frame is presented by a number of previous works (Badhwar et al. 1977; Stephens and Badhwar 1981; Dermer 1986a). Using this formulation, we can estimate the probability of producing pions with four momentum p'_π in this frame. Next, we transform again the coordinate to the fluid-rest frame and obtain the differential cross section of pion production in the fluid-rest frame.

Let us begin with transforming the fluid-rest frame to the rest frame of particle 1. We choose $x - y$ plane so that the particles 1 and 2 moves in this plane. We also choose x axis to be aligned with the direction of velocity of particle 1. In fluid-rest frame, the particle 2 collide with particle 1 with angle θ . In the rest frame of particle 1, this angle becomes θ' . Pions are produced as a result of this collision with zenith angle α' and azimuthal angle ϕ' . Here we choose $\alpha' = 0$ axis to be aligned with the direction of velocity of particle 2 in the rest frame of the particle 1. We also set $\phi = 0$ and π when the pion moves in the $x' - y'$ plane. We show a sketch of the geometry concerning the individual scattering events in Figure 4. The left panel shows the geometry in the fluid-rest frame, while the right panel shows the geometry in the rest frame of particle 1.

In the fluid-rest frame, the four momentum of particle 2 can be expressed as

$$\begin{pmatrix} E_2/c \\ p_{2x} \\ p_{2y} \\ 0 \end{pmatrix} = \begin{pmatrix} m_p c \gamma_2 \\ m_p c \sqrt{\gamma_2^2 - 1} \cos \theta \\ -m_p c \sqrt{\gamma_2^2 - 1} \sin \theta \\ 0 \end{pmatrix}. \quad (43)$$

This is transformed to

$$\begin{aligned} \begin{pmatrix} E'_2/c \\ p'_{2x} \\ p'_{2y} \\ 0 \end{pmatrix} &= \begin{pmatrix} \gamma_1 & -\gamma_1\beta_1 & 0 & 0 \\ -\gamma_1\beta_1 & \gamma_1 & 0 & 0 \\ 0 & 0 & 1 & 0 \\ 0 & 0 & 0 & 1 \end{pmatrix} \begin{pmatrix} m_p c \gamma_2 \\ m_p c \sqrt{\gamma_2^2 - 1} \cos \theta \\ -m_p c \sqrt{\gamma_2^2 - 1} \sin \theta \\ 0 \end{pmatrix} \\ &= \begin{pmatrix} m_p c \gamma_1 (\gamma_2 - \beta_1 \sqrt{\gamma_2^2 - 1} \cos \theta) \\ m_p c \gamma_1 (-\beta_1 \gamma_2 + \sqrt{\gamma_2^2 - 1} \cos \theta) \\ -m_p c \sqrt{\gamma_2^2 - 1} \sin \theta \\ 0 \end{pmatrix}. \end{aligned} \quad (44)$$

Thus, the relation between θ and θ' can be expressed as

$$\tan \theta' = -\frac{p'_{2y}}{p'_{2x}} = \frac{\sqrt{\gamma_2^2 - 1} \sin \theta}{\gamma_1 (-\beta_1 \gamma_2 + \sqrt{\gamma_2^2 - 1} \cos \theta)} \quad (45)$$

In this frame, the differential cross section for pion production can be expressed as (Naito and Takahara 1994)

$$\frac{d\sigma_{pp}(E'_\pi, E'_2)}{dE'_\pi} = \sqrt{E'^2_\pi - m^2_\pi c^4} \int_0^{2\pi} d\phi' \int_{\cos \alpha'_{\max}}^1 d\cos \alpha' \left(E'_\pi \frac{d^3\sigma_{pp}}{dp'^3_\pi c^3} \right), \quad (46)$$

where $\cos \alpha'_{\max} = [\gamma_c E'_\pi - E^*_{\max}(s)] / [\beta_c \gamma_c p'_\pi c]$ ($-1 \leq \cos \alpha'_{\max} \leq 1$), γ_c is the Lorentz factor of the center-of-mass system with respect to the rest frame of particle 1, $E^*_{\max}(s) = (s - 4m^2_p c^4 + m^2_\pi c^4)/2s^{1/2}$ is the energy of pion in the center-of-mass system when the pion obtains the maximum angle α'_{\max} in the rest frame of particle 1 (Dermer 1986b), and s is the Mandelstam variables for s-channel. The estimation of the Lorentz invariant quantum $E'_\pi d^3\sigma_{pp}/dp'^3_\pi c^3$ is explained below.

The four momentum of produced pion in the rest frame of particle 1 can be expressed as

$$p'_\pi = \begin{pmatrix} \sqrt{p'^2_\pi + m^2_\pi c^2} \\ p'_\pi \{ \cos \alpha' \cos \theta' - \sin \alpha' \cos \phi' \sin \theta' \} \\ -p'_\pi \{ \cos \alpha' \sin \theta' + \sin \alpha' \cos \phi' \cos \theta' \} \\ p'_\pi \sin \alpha' \sin \phi' \end{pmatrix}. \quad (47)$$

It can be transformed to the one in the fluid-rest frame as

$$\begin{pmatrix} \gamma_1 & \gamma_1\beta_1 & 0 & 0 \\ \gamma_1\beta_1 & \gamma_1 & 0 & 0 \\ 0 & 0 & 1 & 0 \\ 0 & 0 & 0 & 1 \end{pmatrix} p'_\pi = \begin{pmatrix} \gamma_1 \sqrt{p'^2_\pi + m^2_\pi c^2} + \gamma_1 \beta_1 p'_\pi \{ \cos \alpha' \cos \theta' - \sin \alpha' \cos \phi' \sin \theta' \} \\ \gamma_1 \beta_1 \sqrt{p'^2_\pi + m^2_\pi c^2} + \gamma_1 p'_\pi \{ \cos \alpha' \cos \theta' - \sin \alpha' \cos \phi' \sin \theta' \} \\ -p'_\pi \{ \cos \alpha' \sin \theta' + \sin \alpha' \cos \phi' \cos \theta' \} \\ p'_\pi \sin \alpha' \sin \phi' \end{pmatrix}. \quad (48)$$

Thus, since

$$\int dE_\pi \frac{d\sigma_{pp}(\gamma_1, \gamma_2, \cos \theta)}{dE_\pi} = \int dE'_\pi \frac{d\sigma_{pp}(E'_\pi, E'_2)}{dE'_\pi}, \quad (49)$$

$d\sigma_{pp}(\gamma_1, \gamma_2, \cos \theta)/dE_\pi$ can be expressed as

$$\begin{aligned} \frac{d\sigma_{pp}(\gamma_1, \gamma_2, \cos \theta)}{dE_\pi} &= \frac{d}{dE_\pi} \int \int \int dE'_\pi d\phi' d\cos \alpha' \sqrt{E'^2_\pi - m^2_\pi c^4} \left(E'_\pi \frac{d^3\sigma_{pp}}{dp'^3_\pi c^3} \right) \\ &\quad \times H(\gamma_1 \sqrt{p'^2_\pi + m^2_\pi c^2} + \gamma_1 \beta_1 p'_\pi \{ \cos \alpha' \cos \theta' - \sin \alpha' \cos \phi' \sin \theta' \} - E_\pi) \\ &\quad \times H(E_\pi + dE_\pi - \gamma_1 \sqrt{p'^2_\pi + m^2_\pi c^2} + \gamma_1 \beta_1 p'_\pi \{ \cos \alpha' \cos \theta' - \sin \alpha' \cos \phi' \sin \theta' \}), \end{aligned} \quad (50)$$

where $H(x)$ is the Heaviside function.

Here we explain the formulation to estimate the Lorentz invariant cross section $E'_\pi d^3\sigma_{pp}/dp'^3_\pi c^3$. In the center-of-mass system (labeled as *), the invariant cross section is inferred to have a form (Badhwar et al. 1977; Naito and Takahara 1994)

$$E_\pi^* \frac{d^3\sigma_\pi^*}{d^3p_\pi^*} = \frac{A}{(1 + 4m_p^2 c^4/s)^r} (1 - \tilde{x})^q \exp \left[\frac{Bp_\perp^*}{1 + 4m_p^2 c^4/s} \right], \quad (51)$$

where $\tilde{x} = \{x_\parallel^{*2} + (4/s)(p_\perp^{*2} c^2 + m_\pi^2 c^4)\}^{1/2}$ and $q = (C_1 + C_2 p_\perp^* + C_3 p_\parallel^*)$. Definition of x_\parallel^* is $x_\parallel^* = p_\parallel^* c / \sqrt{s/4 - m_p^2 c^4}$. Here we decompose the momentum of pion in the center-of-mass system of protons into the component which is parallel to the velocity of the protons (p_\parallel^*) and the one which is perpendicular to the velocity (p_\perp^*). The parameters A, B, C_1, C_2, C_3 and r for neutral and charged pions are tabulated in table 1. Note that the Lorentz invariant cross section is expressed in units of $\text{mb}/(\text{GeV}^2/c^3)$, momentum of pion is expressed in units of GeV/c , and energy is expressed in units of GeV . This fitting formula is derived from the study of pp collisions for incident proton energies 6-1500 GeV . Thus we have to note that this formula has to be extrapolated to the high energy range in this study. However, as shown in Naito and Takahara (1994), even if the scaling model is extrapolate to higher energies, they confirmed that the scaling assumption does not much affect the resulting gamma-ray spectrum by comparing their results on the resulting gamma-ray spectrum up to $\sim 10^7$ GeV with the gamma-ray production by the mini-jet model including the QCD effect (Gaisser and Halzen 1987; Berezhinsky et al. 1993). As for the low energy range ($\lesssim 5$ GeV), the isobaric model (Stecker 1971), in which a single pion is produced in a collision, is considered to be better than the scaling model. However, we consider much more energetic protons and the difference between the isobaric model and the scaling model should be unimportant in this study.

2.2.3. Flux of Neutrino and Gamma-ray

The neutral and charged pions decay into gamma-rays, electrons (positrons), and neutrinos as follows:

$$\pi^0 \rightarrow \gamma_1 + \gamma_2 \quad (52)$$

$$\pi^+ \rightarrow \mu^+ + \nu_\mu \rightarrow e^+ + \nu_e + \bar{\nu}_\mu + \nu_\mu \quad (53)$$

$$\pi^- \rightarrow \mu^- + \bar{\nu}_\mu \rightarrow e^- + \bar{\nu}_e + \nu_\mu + \bar{\nu}_\mu. \quad (54)$$

In the case of 2-body decay ($\pi^0 \rightarrow \gamma_1 + \gamma_2$ and $\pi^\pm \rightarrow \mu^\pm + \nu_\mu(\bar{\nu}_\mu)$), the four momentum of gamma-ray and neutrino in the rest frame of the pion can be obtained easily by calculating the conservation of four momentum. As for the 3-body decay ($\mu^\pm \rightarrow e^\pm + \nu_e(\bar{\nu}_e) + \bar{\nu}_\mu(\nu_\mu)$), conservation of four momentum and angular momentum (i.e. spin) have to be taken into account to estimate the resulting energy spectrum of secondary neutrinos in the rest frame of the charged pion. We adopt the formulation presented by Dermer (1986a). It is noted that the distribution of neutrino in the momentum space is, after all, isotropic in the pion rest frame.

Next, we transform the obtained number spectrum of neutrino in the rest frame of pion to the one in the fluid-rest frame. We can transform the number spectrum of neutrinos in pion-rest frame to the one in fluid-rest frame by two steps, that is, Lorentz boost and rotation. Let (θ, ϕ) be the zenith angle and azimuthal angle of pion's velocity in the fluid-rest frame. We set xyz coordinate in the fluid-rest frame and $x''y''z''$ in the pion-rest frame. Here we choose x'' axis to be parallel to the direction of pion's velocity. When the four momentum of neutrino in the pion-rest frame is $(p''_\nu, p''_\nu \cos \alpha'', p''_\nu \sin \alpha'' \cos \beta'', p''_\nu \sin \alpha'' \sin \beta'')$, it is transformed as

$$\begin{pmatrix} E_\nu/c \\ p_{\nu x} \\ p_{\nu y} \\ p_{\nu z} \end{pmatrix} = \begin{pmatrix} 1 & 0 & 0 & 0 \\ 0 & \sin \theta \cos \phi & \cos \theta \cos \phi & -\sin \phi \\ 0 & \sin \theta \sin \phi & \cos \theta \sin \phi & \cos \phi \\ 0 & \cos \theta & -\sin \theta & 0 \end{pmatrix} \begin{pmatrix} \gamma & \gamma\beta & 0 & 0 \\ \gamma\beta & \gamma & 0 & 0 \\ 0 & 0 & 1 & 0 \\ 0 & 0 & 0 & 1 \end{pmatrix} \begin{pmatrix} p''_\nu \\ p''_\nu \cos \alpha'' \\ p''_\nu \sin \alpha'' \cos \beta'' \\ p''_\nu \sin \alpha'' \sin \beta'' \end{pmatrix} \quad (55)$$

Here α'' and β'' are the zenith angle and azimuthal angle of neutrino in the pion-rest frame. It is noted that the zenith angle α'' is defined as the angle between the velocity of neutrino and x'' angle. γ is the Lorentz factor of pion in the fluid-rest frame. From Eq. (55), the energy of neutrino in the fluid-rest frame is expressed as

$$E_\nu/c = \gamma p''_\nu (1 + \beta \cos \alpha''). \quad (56)$$

Thus, by considering the conservation of number of neutrino in the fluid element, the relation

$$\frac{dN_\nu}{dE_\nu} dE_\nu = \int \int \int \int \int dp''_\nu \frac{dn''(p''_\nu)}{dp''_\nu} \frac{d\beta'' \sin \alpha'' d\alpha''}{4\pi} dp_\pi 4\pi p_\pi^2 \frac{d^3 N^\pi}{dp_\pi^3} dE_\nu \delta\{E_\nu - \gamma p''_\nu (1 + \beta \cos \alpha'') c\} \quad (57)$$

can be derived. Here dN_ν/dE_ν is the number spectrum of neutrino [particles GeV^{-1}] in the fluid-rest frame, $dn''(p_\nu'')/dp_\nu''$ is the momentum distribution of a neutrino in the pion-rest frame [$(\text{GeV}/c)^{-1}$], and d^3N^π/dp_π^3 is the number spectrum of pions in the momentum space in the fluid-rest frame [particles $(\text{GeV}/c)^{-3}$]. Finally, the number spectrum of neutrino [particles GeV^{-1}] in the fluid element in the fluid-rest frame can be expressed as

$$\frac{dN_\nu}{dE_\nu} = \frac{1}{2E_\nu} \int \int \int dp_\nu'' \frac{dn''(p_\nu'')}{dp_\nu''} \sin \alpha'' d\alpha'' dp_\pi \frac{dN^\pi}{dp_\pi} \delta \left\{ 1 - \frac{\gamma p_\nu'' (1 + \beta \cos \alpha'') c}{E_\nu} \right\}. \quad (58)$$

It is noted that the number spectrum of pions in the momentum space in the fluid-rest frame is isotropic so that it can be reduced to the number spectrum of pion dN^π/dp_π [particles $(\text{GeV}/c)^{-1}$].

Finally, we transform it to the one in the observer's frame, using the formulation presented in section 2.2.1.

2.3. Detection of Neutrinos

We briefly review the detectability of high energy neutrinos at km^3 detector such as IceCube.

In this study, we adopt the formulation presented by Gaisser and Grillo (1987). The event rate [events s^{-1}] of the neutrino-induced signal whose energy is larger than E_μ at the detector with effective area A_{eff} is estimated as

$$S(\geq E_\mu) = A_{\text{eff}} \int_{E_\mu}^{\infty} dE_\nu \frac{dN_\nu}{dE_\nu} P(E_\nu, E_\mu), \quad (59)$$

where dN_ν/dE_ν is the neutrino energy spectrum [particles $\text{cm}^{-2} \text{s}^{-1} \text{erg}^{-1}$] and $P(E_\nu, E_\mu)$ is the probability that a neutrino aimed at the detector gives a muon with energy above E_μ at the detector. The latter is given by

$$P(E_\nu, E_\mu) = \int_{E_\mu}^{E_\nu} dE_\mu^* \int_{E_\mu^*}^{E_\nu} dE_\mu^{**} \frac{d\sigma}{dE_\mu^{**}} N_A \int_0^\infty dX g(X, E_\mu^*, E_\mu^{**}), \quad (60)$$

where N_A is the Avogadro's number and $g(X, E_\mu^*, E_\mu^{**})$ is the probability that a muon produced with energy E_μ^{**} travels a distance X g cm^{-2} and ends up with energy in $[E_\mu^*, E_\mu^* + dE_\mu^*]$. Gaisser and Grillo (1987) assumed that $g(X, E_\mu^*, E_\mu^{**})$ has a form of

$$g(X, E_\mu^*, E_\mu^{**}) = \frac{\delta(X - X_0)}{\alpha(1 + E_\mu^{**}/\epsilon)}, \quad X_0 = \frac{1}{\beta} \ln \left[\frac{E_\mu^{**} + \epsilon}{E_\mu^* + \epsilon} \right], \quad (61)$$

where $\alpha = 2 \text{ MeV cm}^2 \text{ g}^{-1}$, $\epsilon = 510 \text{ GeV}$, and $\beta = 3.92 \times 10^{-6} \text{ cm}^2 \text{ g}^{-1}$. The cross section $d\sigma/dE_\mu^{**} \text{ cm}^2 \text{ erg}^{-1}$ can be expressed by the differential cross section, which is explained below, as

$$\frac{d\sigma}{dE_\mu^{**}} = \frac{1}{E_\nu} \int_0^1 \frac{\partial^2 \sigma}{\partial x \partial y} dx. \quad (62)$$

The inclusive cross section for the reaction $\mu_\nu + N \rightarrow \mu^- + \text{anything}$ is obtained by the renormalization-group-improved parton model ($N = (n + p)/2$ is the isoscalar nucleon). In this model, the differential cross section is written in terms of the scaling variables $x = Q^2/2M\nu$ and $y = \nu/E_\nu$ as

$$\frac{\partial^2 \sigma}{\partial x \partial y} = \frac{2G_F^2 M E_\nu}{\pi} \left[\frac{M_W^2}{Q^2 + M_W^2} \right]^2 \{xq(x, Q^2) + x(1-y)^2 \bar{q}(x, Q^2)\}, \quad (63)$$

where $-Q^2$ is the invariant momentum transfer between the incident neutrino and outgoing muon, $\nu = E_\nu - E_\mu$ is the energy loss in the laboratory frame, M and M_W are the nucleon and intermediate-boson masses, and G_F is the Fermi constant. As for the distribution function of valence and sea quarks, we adopt the fitting formula (Set 2 with $\Lambda = 290 \text{ MeV}$) presented by Eichten-Hinchliffe-Lange-Quigg (EHLQ) for $x \geq 10^{-4}$ (Eichten et al. 1984; Eichten et al. 1986), while the double-logarithmic approximation (DLA) presented by Reno and Quigg (1988) for $x \leq 10^{-4}$.

3. RESULTS

In this study, when we estimate the flux of neutrinos and gamma-rays from pion decays, we have to check whether the energy spectrum of protons can be regarded to obey the relativistic Maxwellian distribution. In the cases in which energy loss processes are so effective that the energy spectrum of protons do not obey the relativistic Maxwellian distribution any longer, the formulation in this study can not be used and Boltzmann equation should be needed to estimate the proton's energy distribution and resulting flux of neutrinos, which is outscope and next step of this study. Thus, we restrict the situations that meet the following constraints in the *whole* region of the nebula flow. These are: (i) production rate of pions [erg s^{-1}] is much smaller than the luminosity of the pulsar wind. (ii) synchrotron cooling timescale of protons is longer than traveling timescale (defined below) or timescale of pp collisions. (iii) energy transfer timescale from protons to electrons is longer than traveling timescale or timescale of pp collisions (see also the footnotes of table 2).

Here we introduce the definitions of the timescales mentioned above. As for the synchrotron cooling timescale of protons can be written as

$$t_{p,\text{syn}} = \left(\frac{m_p}{m_e}\right)^4 \times t_{e,\text{syn}} \sim 1.1 \times 10^{13} t_{e,\text{syn}}, \quad (64)$$

where $t_{e,\text{syn}}$ is the synchrotron energy loss timescale for an electron and can be written as

$$t_{e,\text{syn}} = 3.9 \times 10 \left(\frac{1 \text{ GeV}}{E}\right) \left(\frac{10^2 \text{ G}}{B}\right)^2 \text{ s}. \quad (65)$$

Traveling timescale, which means the timescale for the bulk flow of the nebula flow to be conveyed to outer region, is defined as

$$t_{\text{travel}} = \frac{r}{v}, \quad (66)$$

where r is the location of the fluid element measured from the pulsar and v is the bulk speed of the nebula flow. Collision timescale between protons is estimated as

$$t_{\text{col}} = \frac{1}{n\sigma_{pp}c}, \quad (67)$$

where n is the number density of protons, σ_{pp} is the cross section of pp interaction, and c is the speed of light. For simplicity, to estimate this timescale, σ_{pp} is set to be 100mb. Collision timescale of energy transfer from protons to electrons is estimated as (Stepney 1983)

$$t_{\text{ep}} = \frac{4}{\ln \Lambda} \frac{n_e}{n_p} \left(\frac{kT_e}{m_e c^2}\right)^2 \frac{1}{n_e \sigma_T c} \quad (68)$$

where σ_T is the Thomson cross section and $\ln \Lambda$ is the value of the Coulomb logarithm which is estimated as

$$\ln \Lambda = \ln \left[\frac{kT_e}{\hbar \omega_p} \right]. \quad (69)$$

Here ω_p is the plasma frequency and is given as

$$\omega_p = \left(\frac{4\pi e^2 c^2 n_e}{3kT_e} \right)^{1/2} \quad (70)$$

for a highly relativistic thermal electron gas (Gould 1981). Here we assume that $T_e = (m_e/m_p)T_p$ and $n_e = n_p$ to estimate the energy transfer timescale, although we found that the energy transfer timescale depends very weakly on their number ratio. In fact, we found that the energy transfer timescale hardly changes even if the number density of electrons becomes $\sim 10^3$ times larger than that of protons.

Some explanations should be added to the constraints (ii) and (iii). We consider that the Maxwellian distribution is hold even if the synchrotron cooling timescale of protons is shorter than the pion production timescale, as long as the traveling timescale is shorter than the synchrotron cooling timescale. This means the flow is conveyed to outer region without losing their energy. It is noted that the definition of the traveling timescale is also frequently used as the timescale of adiabatic cooling. However, effect of adiabatic cooling has been already taken into consideration because we adopt the formulation of nebula flow. Next, we found that the synchrotron cooling timescale of electrons is shorter than the energy transfer timescale from protons to electrons whenever the constraint (iii) is not hold. Thus, in the cases where the constraint (iii) is not hold, most of the energy of protons is considered to be lost through the synchrotron cooling of electrons. Finally, we assume that the energy distribution of protons is hold to be Maxwellian. However, exactly speaking, we should consider another condition, that is, whether the Coulomb collision timescale between protons is sufficiently short that the Maxwellian distribution can be hold. If this condition can not be satisfied, temperature of protons can not be defined exactly and formulation of the nebula flow must be altered by using Boltzmann equation. However, as explained in section 2.1.2, we found in this study that charged and neutral pions are mainly produced just behind the termination shock where the energy distribution of protons obey relativistic Maxwellian. Thus, we think that the order-estimate of the neutrino flux produced by pp collisions will be valid even if the MHD equations are adopted.

Here we show the results. At first, in figure 5, we show contour of the neutrino event whose energy is greater than 10 GeV per year for a km^3 detector of high-energy neutrinos as functions of age [yr] of a pulsar and initial bulk Lorentz factor of the pulsar wind (Models A2-A9, B2-B9, and C2-C9). The pulsar is assumed to be located 10 kpc away from the earth. The amplitude of the magnetic field and period of the pulsar are assumed to be 10^{12}G and 1ms. It is noted that the spin down age is about 2×10^2 yr, so that the range of the age is limited to be within 10^2 yr. Also, when the age of the pulsar is about 10^{-1} yr (Models D4-D9), synchrotron cooling timescale is so short that the condition (ii) is not satisfied (see table 2). As for Model D3, collision timescale between protons is the fastest one and the condition (i) is not satisfied. As for the bulk Lorentz factor of the initial pulsar wind, the maximum value is determined by Eq.(28). When the bulk Lorentz factor is about 10^1 , the energy transfer timescale from protons to electrons are too short (see table 2).

Figure 6 is same with figure 5, but horizontal line represents the initial bulk Lorentz factor of pulsar wind with the age of the pulsar fixed as 1 (Models C2-C9), 10^1 (Models B2-B9), and 10^2yr (Models A2-A9). The reason for the event rate to become smaller for the case of large initial Lorentz factor is, as shown in figure 7, that the number density of protons behind the termination shock becomes smaller. Also, the reason for the event rate to become

smaller for the case of the Lorentz factor to be smaller than 10^4 is that high energy protons do not exist and high energy neutrinos are not produced. It is noted that the cross section between neutrino and quark is roughly proportional to energy of neutrinos in the quark-rest frame.

Figure 7 represents the density (solid line) and temperature (dashed line) behind the termination shock as a function of the initial bulk Lorentz factor of the pulsar wind. The amplitude of the magnetic field, period, and age of the pulsar are assumed to be 10^{12}G , 1ms , and 10^2yr (Models A2-A9). As mentioned above, the number density of protons is smaller for the larger initial bulk Lorentz factor. We can also confirm that the temperature of protons behind the termination shock wave is roughly same with the initial kinetic energy of the protons.

The reason why the flux of neutrinos becomes larger with time can be understood by figure 8. Figure 8 shows profiles of velocity, number density of protons, temperature, magnetic field, and emissivity of charged pions in units of $[10^{-20}\text{erg s}^{-1} \text{cm}^{-3}]$ and $[10^{-20}\text{particles s}^{-1} \text{cm}^{-3}]$. The inner and outer boundaries correspond to the location of the termination shock wave and the innermost region of the surrounding supernova remnant. The amplitude of the magnetic field and period of the pulsar are assumed to be 10^{12}G and 1ms . The left panel represents the case that the age of the pulsar is 1yr (Model C5), while the right panel shows the case that the age of the pulsar is 10^2yr (Model A5). In both cases, initial bulk Lorentz factor of the pulsar wind is set to be 10^5 . The pressure of the innermost region of the remnant becomes smaller with time (see figure 2). Thus the location of the termination shock moves inward with time, which results in higher density and higher emissivity of neutrinos. Also, additionally, the radius of the remnant becomes outward, which results in the region of the nebula flow becomes larger with time. These are the reason why the flux of neutrinos becomes larger with time. We can also find that the emissivity of charged pions $[\text{particles cm}^{-3} \text{s}^{-1}]$ in the nebula flow can be roughly estimated as

$$\epsilon = n^2 c \sigma_{pp} = 3 \times 10^{-5} \left(\frac{n}{10^5 \text{cm}^{-3}} \right)^2 \left(\frac{\sigma_{pp}}{100 \text{mb}} \right). \quad (71)$$

For example, in the left panel of figure 8, the density and emissivity just behind the termination shock are about $10^5 [\text{cm}^{-3}]$ and $10^{-5} [\text{particles cm}^{-3} \text{s}^{-1}]$, respectively. Also, those values just forward the innermost region of the surrounding supernova remnant are about $1 [\text{cm}^{-3}]$ and $10^{-14} [\text{particles cm}^{-3} \text{s}^{-1}]$, respectively. Thus the emissivity can be roughly reproduced by using Eq. (71), although the emissivity is obtained by using formulation presented in section 2.2.1. This means the rough estimate holds a good approximation even if the protons obey the Maxwellian distribution. Also, as pointed out in section 2.1.2, we can find that pions are mainly produced just behind the termination shock.

Before we go to the further discussion, we consider the proper value for the bulk Lorentz factor of the pulsar wind by introducing the Goldreich-Julian value, which is usually used to estimate the charge density of the e^+e^- pair plasma, although the initial bulk Lorentz factor of the pulsar wind is treated as a free parameter in figure 7. Goldreich-Julian value at the equatorial plane at radius r can be written as

$$n_{\text{GJ}}(r) = \frac{\vec{B}(r) \cdot \vec{\Omega}}{2\pi ec} = \frac{B\Omega}{2\pi ec} = 6.9 \times 10^{-2} \frac{B(r)}{P} \text{ cm}^{-3}, \quad (72)$$

where $B(r)$ is the amplitude of the magnetic field at radius r in a unit of G, Ω is the angular velocity of a pulsar, and P is the period of the pulsar in a unit of sec. Assuming that the magnetic field around the pulsar is dipole, Eq.(72) can be written as

$$n_{\text{GJ}}(r) = 6.9 \times 10^{13} \left(\frac{1\text{ms}}{P} \right) \left(\frac{B_p}{10^{12}\text{G}} \right) \left(\frac{10^6\text{cm}}{r} \right)^3 \text{ cm}^{-3}, \quad (73)$$

where B_p is the amplitude of the magnetic field at the pole of the pulsar. Since the location of the light cylinder is

$$R_{\text{lc}} = 4.8 \times 10^6 \left(\frac{P}{1\text{ms}} \right) \text{ cm}, \quad (74)$$

the Goldreich-Julian value at the light cylinder can be expressed as

$$n_{\text{GJ}}(R_{\text{lc}}) = 6.4 \times 10^{11} \left(\frac{1\text{ms}}{P} \right)^4 \left(\frac{B_p}{10^{12}\text{G}} \right) \text{ cm}^{-3}. \quad (75)$$

From this value, we can estimate the net number density of electrons ($|n(e^+) - n(e^-)|$) in the pulsar wind just ahead of the termination shock as

$$n(r_s) = \left(\frac{R_{\text{lc}}}{r_s} \right)^2 n_{\text{GJ}}(R_{\text{lc}}) \text{ cm}^{-3}, \quad (76)$$

where we use the conservation law of number flux of protons, $4\pi R_{\text{lc}}^2 \Gamma n_{\text{GJ}}(R_{\text{lc}}) = 4\pi r_s^2 \Gamma n(r_s)$. Eq.(76) can be written by inserting Eq.(75) as

$$n(r_s) = 1.5 \times 10 \left(\frac{1\text{ms}}{P} \right)^2 \left(\frac{B_p}{10^{12}\text{G}} \right) \left(\frac{10^{12}\text{cm}}{r_s} \right)^2 \text{ cm}^{-3}. \quad (77)$$

The location of the termination shock is found to be $\sim 10^{12}$ cm from figure 8. On the other hand, the number density of protons can be estimated by using relation $L \sim 4\pi n \Gamma^2 r_s^2 m_p c^3$ (see Eqs.(2) and (29). note that σ is much smaller than unity and bulk flow is highly relativistic). It can be expressed as

$$n(r_s) = 1.7 \times \left(\frac{10^5}{\Gamma} \right)^2 \left(\frac{10^{12}\text{cm}}{r_s} \right)^2 \left(\frac{B_p}{10^{12}\text{G}} \right)^2 \left(\frac{1\text{ms}}{P} \right)^4 \left(\frac{R}{10^6\text{cm}} \right)^6 \text{ cm}^{-3}. \quad (78)$$

By comparing Eq.(77) with Eq.(78) and assuming that number density of proton is comparable with the net number density of electrons ($|n(e^+) - n(e^-)|$), proper value for the bulk Lorentz factor seems to be $\Gamma \sim 10^4 - 10^5$.

In figure 9, we show spectrum of energy fluxes of neutrinos from a pulsar which is located 10kpc away from the earth. The amplitude of the magnetic field and period of the pulsar is assumed to be 10^{12}G and 1ms. The detection limits of the energy flux for AMANDA-B10, AMANDA II (1yr), and IceCube are represented by horizontal lines. The atmospheric neutrino energy fluxes for a circular patch of 1° are also shown (Honda et al. 1995). The left panel represents the case that the age of the pulsar is 1yr (Models C2-C9), while right panel represent the case that the age is 10^2yr (Models A2-A9). From this figure, we can find that there is a possibility to detect the signals of neutrinos from pulsar winds in our galaxy.

In figure 10, we show neutrino event rate per year from the nebula flow considered in figure 9 as a function of the muon energy threshold in a km^3 high-energy neutrino detector. The left panel represents the case that the age of the pulsar is 1yr (Models C2-C9), while right panel represent the case that the age is 10^2yr (Models A2-A9). The event rates expected of atmospheric neutrino for a circular patch of 1° are also shown (Honda et al. 1995). The event rates are shown for the vertical downgoing atmospheric neutrinos and horizontal ones. It is confirmed that there is a possibility that the signals from the nebula flow dominates the background of atmospheric neutrinos.

For comparison, in figure 11, we show the spectrum of energy fluxes of neutrinos from a pulsar of which the amplitude of the magnetic field and period are assumed to be 10^{12}G and 5ms. Location of the pulsar is assumed to be 10 kpc away from the earth. The left panel represents the case that the age of the pulsar is 10yr (Models G1-G8), while right panel represents the case that the age is 10^3yr (Models E1-E8). In these cases, the fluxes of neutrinos are much lower than the atmospheric neutrinos and detection limits of km^3 high-energy neutrino detectors. We can conclude that the detectability of the signals from the pulsar winds strongly depends on the period of the pulsar, which reflects the luminosity of the pulsar winds (see Eq.(29)).

We check the reason why the flux of neutrinos becomes lower for the case where period of the pulsar is 5ms. Figure 12 shows profiles of velocity, number density of protons, temperature, magnetic field, and emissivity of charged pions in units of $[10^{-20}\text{erg s}^{-1} \text{cm}^{-3}]$ and $[10^{-20}\text{particles s}^{-1} \text{cm}^{-3}]$. The left panel represents the case that the period and age of the pulsar are 1ms and 10^2 yr (Model A5; same with the right panel of figure 8), while the right panel shows the case that the period and age of the pulsar are 5ms and 10^3 yr (Model E5). In both cases, initial bulk Lorentz factor of the pulsar wind is set to be 10^5 . In the latter case, the location of the termination shock must be outward compared with the former in

order to achieve the pressure balance between the outermost region of the nebula flow and innermost region of the remnant. This is because luminosity of the pulsar wind and the pressure behind the termination shock are lower in the latter case. That is why the density of behind the termination shock is lower in the latter case and results in lower emissivity of neutrinos.

Here we consider the detectability of gamma-rays from neutral pions. In figure 13, integrated gamma-ray fluxes from the neutral pion decays are shown assuming that the supernova ejecta has been optically thin for gamma-rays (Matz et al 1988). The amplitude of the magnetic field and period of the pulsar are assumed to be 10^{12} G and 1ms. The left panel represents the case that the age of the pulsar is 1yr (Models C2-C9), while the right panel shows the case that the age of the pulsar is 10^2 yr (Models A2-A9). The detection limits of integrated fluxes for GLAST, STACEE, CELESTE, HEGRA, CANGAROO, MAGIC, VERITAS, and H.E.S.S. are also shown. From these figures, we can find that there is a possibility to detect gamma-rays from decays of neutral pions by these telescopes. As for the spectrum of gamma-rays from electrons, it is difficult to estimate it because we have to solve time evolution of energy distribution of electrons taking into account the effects of cooling processes such as synchrotron emission, inverse compton, and pair annihilation as well as heating process such as Coulomb collisions between electrons and protons and pair creations. This is difficult to solve and we regard it as a future work.

On the other hand, we show the same figures in figure 14 but for the case that the period of the pulsar is 5ms. The left panel represents the case that the age of the pulsar is 10yr (Models G1-G8), while the right panel shows the case that the age of the pulsar is 10^3 yr (Models E1-E8). In these cases, the flux of gamma-rays is too low to detect.

Finally, it is noted that there are some cases in which the location of the termination shock is driven back to the surface of the neutron star since the pressure balance can not be achieved (see section 2.1.3). Models H2 and H3 are the case (see table 2). In these cases, the density behind the shock is so large that the resulting flux of neutrino is very high. There will be a tendency that the reverse shock is likely to be driven back to the surface of the neutron star when the age of the pulsar is young, because the pressure at the innermost region of the remnant is large (see figure 2). Thus there may be a possibility to detect a number of high energy neutrinos from the pulsar wind at the early stage of the supernova explosion, although the protons in the nebula flow will also suffer from synchrotron cooling and/or energy transfer to electrons.

4. DISCUSSIONS

First, we discuss the timescale of energy loss of protons due to the inverse compton (IC) scattering. This timescale depends on the strength of the seed photons that suffers from great uncertainty. However, we can estimate the lower limit of this timescale and show that this process is not so effective. The ratio of the synchrotron cooling timescale of protons relative to IC can be written as

$$\frac{t_{\text{sync}}}{t_{\text{IC}}} = \frac{U_\gamma}{U_B}, \quad (79)$$

where U_γ and U_B are energy density of seed photon and electric-magnetic fields. In the case in which energy transfer from protons to electrons is ineffective, the energy density of seed photon should be smaller than that of electrons as long as the seed photons come from bremsstrahlung and/or synchrotron emission from electrons. Thus, using Eq.(22), the upper limit of the ratio of $t_{\text{sync}}/t_{\text{IC}}$ can be expressed as

$$\frac{t_{\text{sync}}}{t_{\text{IC}}} \leq \frac{U_e}{U_B} = \frac{n_e m_e U_p}{n_p m_p U_B} = \frac{n_e m_e}{n_p m_p} \frac{z^2 \{3\sigma + (3\sigma/z)^{2/3}\}^2}{\sigma \{3\sigma z^2 + (3\sigma)^{2/3} z^{4/3}\}^{4/3} [4 + \{3\sigma + (3\sigma/z)^{2/3}\}^2]}. \quad (80)$$

We show in figure 15 the ratio of the thermal energy of electrons relative to the energy of electric-magnetic fields as a function of z in the case where $n_e = n_p$. Here σ is set to be $\sigma_c = 6.67 \times 10^{-3}$. We can find that the upper limit of the ratio of $t_{\text{sync}}/t_{\text{IC}}$ is smaller than unity as long as $n_e/n_p \lesssim 2 \times 10^2$. That is why we can conclude that IC cooling is not so effective. Here we neglect the contribution of cosmic microwave-background, since it can be expressed by an equivalent field strength $B_{\text{CMB}} = 3.24 \mu\text{G}$, which is sufficiently small and can be neglected. We also check the contribution of the photon field in the supernova remnant around the nebula flow, since a portion of it may be transported into the region of the nebula flow. The energy density of the photon field in the supernova remnant can be estimated from figure 2 and expressed by equivalent field strength $B_{\text{SN}} \sim 3.9 \text{ G}, 1.3 \times 10^{-1} \text{ G}, 4.1 \times 10^{-3} \text{ G},$ and $1.6 \times 10^{-4} \text{ G}$ for $t = 1, 10, 10^2,$ and 10^3 yr . These values are also smaller than strength of the magnetic fields in almost all cases (see figures 8 and 12). We should also estimate the number density of photons from surface of the pulsar. The temperature of the surface of the neutrons star is considered to become in the range ($10^6 - 10^7$) K about 1 yr after the explosion, although there are some uncertainties of the cooling processes (Slane et al. 2002). Thus the energy density of the photon field at radius r can be estimated as

$$U_{\gamma, \text{pulsar}} = \frac{4\pi R^2 \sigma T^4}{4\pi r^2 c}, \quad (81)$$

where R is the radius of the pulsar and σ is the Stefan-Boltzmann constant. Eq. (81) can be expressed by the equivalent field strength as

$$B_{\text{pulsar}} = 2.2 \times 10 \left(\frac{R}{10^6 \text{cm}} \right) \left(\frac{T}{10^7 \text{K}} \right) \left(\frac{10^{12} \text{cm}}{r} \right) \text{ G}, \quad (82)$$

which is also smaller than strength of the magnetic fields in almost all cases (see figures 8 and 12).

Next, we consider the effect of synchrotron cooling of muons and pions. As for the mean life time of muon in the rest frame is 2.197×10^{-6} s and that of charged pion is 2.603×10^{-8} s. Since synchrotron cooling time of muon is

$$\begin{aligned} t_{\mu,\text{syn}} &= \left(\frac{m_\mu}{m_e}\right)^4 \times t_{e,\text{syn}} \sim 1.82 \times 10^9 t_{e,\text{syn}} \\ &= 7.11 \times 10^{10} \left(\frac{1 \text{ GeV}}{E_\mu}\right) \left(\frac{10^2 \text{ G}}{B}\right)^2 \text{ s}, \end{aligned} \quad (83)$$

the condition that the synchrotron cooling time becomes shorter than that of the mean life time in the fluid rest frame can be expressed as

$$E_\mu \geq 5.85 \times 10^5 \left(\frac{10^4 \text{ G}}{B}\right) \text{ GeV}. \quad (84)$$

Since the amplitude of the magnetic field in the nebula flow becomes $\sim 10^4$ G at most (see figures 8 and 12), the energy spectrum of neutrinos whose energy is larger than $\sim 10^5$ GeV may be modified due to the effect of the synchrotron cooling of muons. Similarly, the energy spectrum of neutrinos whose energy is larger than $\sim 10^7$ GeV may be modified by the effect of synchrotron cooling of charged pions.

Third, we discuss the cooling process due to photopion production which is interesting and should be investigated in detail in the forth-coming paper because this is another process of producing pions and may make the flux of neutrinos and gamma-rays enhance. Here we give the rough estimation for this effect. The source of the seed photons are considered to be the synchrotron photons emitted by electrons, the photon field in the supernova remnant around the nebula flow, and photons from surface of the pulsar. The typical frequency of the synchrotron photon is (Rybicki and Lightman 1979)

$$\nu \sim 0.29 \times \frac{3}{8\pi} \gamma^2 \frac{eB}{m_e c} \sim 6.1 \times 10^5 \gamma^2 \left(\frac{B}{1\text{G}}\right), \quad (85)$$

where γ is the Lorenz factor of electrons in the fluid rest frame and is considered to be almost same with the initial bulk Lorenz factor of the pulsar wind ($\equiv \Gamma$) as long as the electrons do not lose their energy by synchrotron cooling. Here the average angle between the magnetic field and direction of motion of electron is set to be $\pi/4$. This frequency corresponds to the energy

$$E_\nu = 2.5 \times 10^{-9} \gamma^2 \left(\frac{B}{1\text{G}}\right) \text{ eV}. \quad (86)$$

Since there is a large peak in the photopion production cross section at $\epsilon \sim 0.35m_p c^2$ at the rest frame of a proton and the width of the peak cross section is also $\Delta\epsilon \sim 0.2\text{GeV}$ (Stecker 1979), the energy of protons in the fluid rest frame which interact with the seed photons can be expressed as

$$E_p \sim \frac{0.35m_p^2 c^4}{E_\nu} = 1.2 \times 10^{13} \gamma^{-2} \left(\frac{10^4 \text{G}}{B} \right) \text{ GeV}. \quad (87)$$

This shows, to be sure, that the protons in the nebula flow cause the photopion interactions when the initial bulk Lorentz factor of the pulsar wind is larger than $\sim 10^5$. We roughly estimate the upper limit of the contribution of photopion production relative to pp interaction. The maximum number density of photons by synchrotron emission is estimated as

$$\begin{aligned} n_{\gamma,\text{sync}} &\leq \frac{U_e}{E_\nu} = \frac{n_e m_e U_p}{n_p m_p E_\nu} \\ &\sim \frac{m_e m_p c^2 \Gamma n_e}{m_p E_\nu} = 2.0 \times 10^5 \left(\frac{10^5}{\Gamma} \right) \left(\frac{10^4 \text{G}}{B} \right) n_e. \end{aligned} \quad (88)$$

Thus, if we assume that the energy loss rate per interaction is same between photopion production and pp interaction, and assume that the cross section of photopion production is constant ($\sim 5 \times 10^{-28} \text{cm}^2$), the contribution of photopion production relative to pp interaction ($\sim 10^{-25} \text{cm}^2$) can be estimated to be

$$\frac{\sigma_{p\gamma} n_{\gamma,\text{sync}}}{\sigma_{pp} n_p} \sim 1.0 \times 10^3 \left(\frac{10^5}{\Gamma} \right) \left(\frac{10^4 \text{G}}{B} \right) \left(\frac{n_e}{n_p} \right). \quad (89)$$

In reality, as mentioned above, there is a large peak in the photopion production cross section at the photon energy $\epsilon = 0.35m_p c^2$ in the proton rest frame due to the $\Delta(1232)$ resonance (Stecker 1979; Waxman and Bahcall 1997; Amato et al. 2003). Thus the contribution of photopion production would be much smaller than the estimated value in Eq.(89) in the case that the typical energy of protons which interact with the synchrotron photons from electrons through the $\Delta(1232)$ resonance is much different from the mean energy of protons in the fluid. We emphasize again that we estimated here just the upper limit of the contribution of photopion production. Also, it is noted here that the synchrotron cooling time of electrons can be estimated as

$$t_{e,\text{sync}} = 7.6 \times 10^{-5} \left(\frac{10^5}{\Gamma} \right) \left(\frac{10^4 \text{G}}{B} \right)^2 \text{ s}. \quad (90)$$

Thus, even if the effect of the photopion production can not be neglected, it will be effective only within a very short distance from the location of the termination shock. As for the

contribution of the photon field from the supernova remnant, the energy of protons that interacts with the photon field can be estimated as

$$E_p \sim \frac{0.35m_p^2c^4}{kT_\gamma} \sim 3.1 \times 10^9 \left(\frac{0.1\text{eV}}{kT_\gamma} \right) \text{ GeV}, \quad (91)$$

where T_γ is the temperature of the photon field. Thus the required energy for a proton to interact with the photon field from the supernova remnant seems to be too high. As for the contribution of the photon field from the pulsar, the number density of the photon field can be expressed as

$$\begin{aligned} n_{\gamma,\text{pulsar}} &= \frac{4\pi R^2 \sigma T^4}{4\pi r^2 c} \left(\frac{1}{kT} \right) \\ &= 1.4 \times 10^{10} \left(\frac{10^{12}\text{cm}}{r} \right)^2 \left(\frac{R}{10^6\text{cm}} \right)^2 \left(\frac{T}{10^7\text{K}} \right)^3 \text{ cm}^{-3}. \end{aligned} \quad (92)$$

Thus, from Eqs.(88) and (92), the photon fields from the pulsar can dominate the synchrotron photons. As for the energy of protons that interacts with the photon field, it can be estimated as

$$E_p \sim 3.6 \times 10^5 \left(\frac{10^7\text{K}}{T} \right) \text{ GeV}. \quad (93)$$

Thus, protons with energies $\sim 10^5$ GeV may interact with the photons from the pulsar and produce much more pions than estimated in this study. Thus, the spectrum of neutrinos and gamma-rays around $\sim 10^5$ GeV may be modified and intensity may be enhanced due to this effect. This effect is very important and should be investigated carefully in the very near future.

In this study, we consider the pion production due to pp interaction. However, in many cases, total energy of colliding protons in their center-of-mass system exceeds the experimental limit. Moreover, it exceeds the mass of the top quark ($m_t = 174.3 \pm 5.1\text{GeV}$ from direct observation of top events, and $m_t = 178.1_{-8.3}^{+10.4}\text{GeV}$ from standard model electroweak fit (Hagiwara et al. 2002)). As explained in section 2.2.2, it is confirmed that the scaling assumption does not much affect the resulting gamma-ray spectrum by comparing the resulting gamma-ray spectrum up to $\sim 10^7$ GeV with the gamma-ray production by the mini-jet model including the QCD effect even if the scaling model is extrapolate to higher energies. However, it should be confirmed whether the scaling assumption is still valid at more high energies, which is investigated in the near future.

In this study, we have estimated the energy transfer timescale assuming that it is mainly caused by Coulomb scattering between protons and electrons (Stepney 1983). In this case,

the energy transfer timescale depends very weakly on the number ratio of protons to electrons (positrons), as shown in section 3. However, it is pointed out by Hoshino et al. (1992) that the efficiency of the energy transfer from protons to positrons may be higher than that from protons to electrons due to the effect of cyclotron resonance. Thus, if this process is really effective and determines the energy transfer rate, number ratio of protons to electrons (positrons) should be important because the energy transfer timescale will strongly depend on the number ratio. Also, the expected flux of neutrinos and gamma-rays from pp interactions will be decreased than estimated in this study. In this case, however, emission of gamma-rays from electron-positron plasma should be important through the process of synchrotron, inverse compton, and pair annihilation. Neutrino emission from electron-positron plasma is also expected from electron-positron pair annihilation. In more realistic cases, there will be heavy nuclei in the pulsar wind, which should be taken into account as a next step of this study. In this case, hadronic interactions should be enhanced since heavy nuclei are composed of protons and neutrons and baryon number should be enhanced. In order to obtain the contribution of heavy nuclei, photodisintegration of heavy nuclei should be also taken into account, which will make the situation rather complicated.

In this study, we assumed that the pressure balance is hold at the interface between the nebula flow and supernova remnant. Also, we fixed the fraction of magnetic field energy in the pulsar wind so that the velocity of the nebula flow is almost same with that of the supernova remnant at the interface, which makes the location of the termination shock fixed. However, in reality, the pressure balance should not be always hold and velocity of the nebula flow and supernova remnant will be different in general. This means that we need to consider the momentum transfer between the nebula flow and supernova remnant, which will change profiles of density, temperature, and amplitude of the magnetic field in the nebula flow. This is a future work and it may require numerical calculations. Also, it is assumed that the system is spherical symmetry for simplicity. Of course, in reality, we should consider the effects of geometrical anisotropy of the system (Hester et al. 2002).

In this study, we investigated the effects that bulk Lorentz factor is dissipated into the random motion of the charged particles when they pass through the termination shock. Of course, a part of charged particles will be accelerated at more high energies due to Fermi acceleration (Blandford and Ostriker 1978). Maximum energy of protons due to Fermi acceleration can be estimated using Larmor radius as

$$E_{\max} = 3.3 \times 10^9 \left(\frac{B}{10^4 \text{G}} \right) \left(\frac{r}{10^{12} \text{cm}} \right) \text{ GeV}. \quad (94)$$

From figures 8 and 12, E_{\max} will be about 10^9 GeV and 10^8 GeV for the cases of $P = 1\text{ms}$ and 5ms (B_p is set to be 10^{12}G). Thus, the flux and mean energies of neutrinos and gamma-rays may be enhanced due to the effects of Fermi acceleration. We will have to investigate

carefully how much of charged particles are accelerated by Fermi acceleration in order to estimate this effects quantitatively.

It is noted that the ν_τ is generated due to the effect of neutrino oscillation (Fukuda et al. 1998). The scale length for ν_μ with energy E_ν to be converted to be ν_τ due to the vacuum oscillation is written as

$$L = 4.9 \times 10^{10} \left(\frac{E_\nu}{10^3 \text{GeV}} \right) \left(\frac{2.5 \times 10^{-3} \text{eV}^2}{\Delta m^2} \right) \text{ cm}, \quad (95)$$

where Δm is the mass difference between m_2 and m_3 . Thus the neutrinos produced in the nebula flow are well mixed and ratios of the flux among three flavors (e , μ , and τ) will become order unity at the earth. Thus there may be a possibility to detect the double-bang events (a big hadronic shower from the initial ν_τ interaction and a second big particle cascade due to τ decay, which was pointed out by Learned and Pakvasa 1995) at the km^3 neutrino telescopes from the system investigated in this study.

At present, there is no candidate of a pulsar whose wind is more luminous than $\sim 10^{43}$ erg s^{-1} like the case of $B = 10^{12}\text{G}$ and $P = 1\text{ms}$ in our galaxy (Manchester et al. 1999; Torres and Nuza 2003). This is consistent with the fact that there is no point-like source detected at AMANDA-B10 detector (Ahrens et al. 2003). We hope that such point-like sources are found at AMANDA-II and/or IceCube detectors in the near future. Also, we hope that such an active pulsar is found by pulsar surveys in radio, X-ray, and gamma-ray bands. We also hope that a newly born supernova will appear in our galaxy in the near future.

Recently, Granot and Guetta (2003) pointed out the possibility to detect neutrinos from pulsar nebula that is associated with a gamma-ray burst (GRB). It will be interesting to apply our model to GRB scenario and estimate fluxes of neutrino background by setting the amplitude of magnetic field at the pole of the pulsar is set to be (10^{14} - 10^{15}) G (Granot and Guetta 2003). Information on GRB formation rate history and explosion mechanism of GRB may be obtained if such signals are detected (Nagataki et al. 2003a; Nagataki et al. 2003b).

5. SUMMARY AND CONCLUSION

In this study, we have estimated fluxes of neutrinos and gamma-rays that are generated from decays of charged and neutral pions from a pulsar surrounded by supernova ejecta in our galaxy, including an effect that has not been taken into consideration, that is, interactions between high energy cosmic rays themselves in the nebula flow, assuming that hadronic

components be the energetically dominant species in the pulsar wind. Bulk flow is assumed to be randomized by passing through the termination shock and energy distribution functions of protons and electrons behind the termination shock obey the relativistic Maxwellians.

We have found that fluxes of neutrinos and gamma-rays depend very sensitively on the wind luminosity, which is assumed to be comparable with the spin-down luminosity. In the case where $B = 10^{12}\text{G}$ and $P = 1\text{ms}$, neutrinos should be detected by km^3 high-energy neutrino detectors such as AMANDA and IceCube. Also, gamma-rays should be detected by Cherenkov telescopes such as CANGAROO and H.E.S.S. as well as by gamma-ray satellites such as GLAST. On the other hand, in the case where $B = 10^{12}\text{G}$ and $P = 5\text{ms}$, fluxes of neutrinos will be too low to be detected even by the next-generation detectors. However, even in the case where $B = 10^{12}\text{G}$ and $P = 5\text{ms}$, there is a possibility that very high flux of neutrinos and gamma-rays may be realized at the early stage of a supernova explosion ($t \leq 1\text{yr}$), where the location of the termination shock is very near to the pulsar (ex. Model H3 and H4 in table 2). We also found that there is a possibility that protons with energies $\sim 10^5$ GeV in the nebula flow may interact with the photon field from surface of the pulsar and produce much pions, which enhances the intensity of resulting neutrinos and gamma-rays.

We have found that interactions between high energy cosmic rays themselves are so effective that this effect can be confirmed by future observations. Thus, we conclude that it is worth while investigating this effect further in the near future.

The author thanks K. Sato, M. Hoshino, S. Shibata, S. Yamada, S. Yoshida, T. Naito, and K. Kohri for useful comments. The author is also pleased to acknowledge useful comments by the anonymous referee of this manuscript. This work is supported in part by Grants-in-Aid for scientific research provided by the Ministry of Education, Science and Culture of Japan through Research Grant No.S 14102004 and No. 14079202.

A. Estimation of the Adiabatic Index

According to Hoshino et al. (1992), the distribution functions of protons behind the termination shock are almost exactly described by relativistic Maxwellians as

$$N(\gamma) = A\gamma \exp \left[-\frac{m_p c^2}{k_B T} (\gamma - 1) \right], \quad (\text{A1})$$

where k_B is the Boltzmann constant and A is the normalization factor in units of cm^{-3} . In this case, the number density (n) [cm^{-3}], energy density (e) [erg cm^{-3}], and pressure (P)

[dyn cm⁻²] can be written as

$$n = Ae^\alpha \int_1^\infty \gamma e^{-\alpha\gamma} d\gamma = A \left[\frac{1}{\alpha} + \frac{1}{\alpha^2} \right], \quad (\text{A2})$$

$$\begin{aligned} e &= \int E \left(\frac{dn}{d^3x d^3p} \right) d^3p = \int m_p c^2 \gamma \frac{N(\gamma)}{4\pi p^2 \frac{dp}{d\gamma}} 4\pi p^2 \frac{m_p c \gamma}{\sqrt{\gamma^2 - 1}} d\gamma = Am_p c^2 e^\alpha \int_1^\infty \gamma^2 e^{-\alpha\gamma} d\gamma \\ &= Ak_B T \left[1 + \frac{2}{\alpha} + \frac{2}{\alpha^2} \right], \end{aligned} \quad (\text{A3})$$

and

$$\begin{aligned} P &= \frac{1}{3} \int p v \left(\frac{dn}{d^3x d^3p} \right) d^3p = \frac{1}{3} \int p \frac{pc^2}{E} \frac{N(\gamma)}{4\pi p^2 \frac{dp}{d\gamma}} 4\pi p^2 dp = \frac{Am_p c^2}{3} e^\alpha \int_1^\infty (\gamma^2 - 1) e^{-\frac{m_p c^2}{k_B T} \gamma} d\gamma \\ &= \frac{2}{3} Ak_B T \left[\frac{1}{\alpha} + \frac{1}{\alpha^2} \right], \end{aligned} \quad (\text{A4})$$

where $\alpha = m_p c^2 / k_B T$, $E = m_p c^2 \gamma$, $dn/d^3x d^3p$ is the number density in phase space. In this case, the relation $P = 2nk_B T/3$ holds exactly, and in the high temperature limit ($\alpha \ll 1$), the relation

$$E = eV = 3PV \quad (\text{A5})$$

holds approximately, where V is the volume [cm³]. In this case, the relation $3VdP = -4PdV$ holds in the adiabatic transition. Thus $P \propto V^{-4/3} \propto \rho^{4/3}$ and adiabatic index becomes 4/3 in high temperature limit.

B. Derivation of Number Flux of Pions in Observer's Frame

We consider an fluid element and number spectrum of pions produced in the fluid element. Using the number spectrum of pions per solid angle [particles s⁻¹ erg⁻¹ sr⁻¹], the conservation law of number of particles can be expressed as

$$\int dE_\nu \int \sin \theta d\theta d\phi \frac{1}{4\pi} F(E_\nu) dt = \int d\bar{E}_\nu \int \sin \bar{\theta} d\bar{\theta} d\bar{\phi} \frac{d}{d\Omega} \bar{F}(\bar{E}_\nu) dt \bar{\Gamma} (1 - \bar{\beta} \cos \bar{\theta}), \quad (\text{B1})$$

where bars are labeled for the quantum of the observer's frame, while the quantum without label denote the ones in the fluid-rest frame. The axis $\theta = \bar{\theta} = 0$ is set to be aligned with the direction of the observer (i.e. the earth) measured from the fluid element. $\bar{\Gamma}$ is the bulk Lorentz factor of the fluid element in the observer's frame. It is noted that $dt_A = \bar{\Gamma} (1 - \bar{\beta}) dt$

is the time interval of the radiation as received by a stationary receiver in the observer's frame (Rybicki and Lightman 1979). Here we define the quantum $N(\theta)$ as

$$N(\theta) = \int dE_\nu F(E_\nu) \text{ [particles s}^{-1}\text{]}. \quad (\text{B2})$$

Using this expression, the relation

$$\frac{d}{d\Omega} \bar{N}(\bar{\theta}) = \frac{1}{\bar{\Gamma}(1 - \bar{\beta} \cos \bar{\theta})} \frac{\sin \theta}{\sin \bar{\theta}} \frac{d\phi}{d\bar{\phi}} \frac{1}{4\pi} N(\theta) \quad (\text{B3})$$

can be derived. Using the relation $\cos \bar{\theta} = (\cos \theta + \beta)/(1 + \beta \cos \theta)$ and $d\phi = d\bar{\phi}$, Eq. (B3) can be expressed as

$$\frac{d}{d\Omega} \bar{N}(\bar{\theta}) = \frac{1}{\bar{\Gamma}^3} \frac{1}{(1 - \bar{\beta} \cos \bar{\theta})^3} \frac{1}{4\pi} N(\theta). \quad (\text{B4})$$

Also, the relation $\bar{F}(\bar{E}_\nu) = F(E_\nu) dE_\nu / d\bar{E}_\nu$ can be expressed as

$$\bar{F}(\bar{E}_\nu) = \frac{1}{\bar{\Gamma}(1 + \bar{\beta} \cos \theta)} F(E_\nu) = \bar{\Gamma}(1 - \bar{\beta} \cos \bar{\theta}) F(E_\nu). \quad (\text{B5})$$

Finally, using Eqs. (B4) and (B5), the relation

$$\frac{d}{d\Omega} \bar{F}(\bar{E}_\nu) = \frac{1}{\bar{\Gamma}^2(1 - \bar{\beta} \cos \bar{\theta})^2} \frac{1}{4\pi} F(E_\nu) \quad (\text{B6})$$

is derived.

C. Analytical Solution for the Nebula Flow

The analytical solution of equations for the nebula flow is obtained by Kennel and Coroniti (1984), which is expressed as

$$(1 + u_2^2 v^2)^{1/2} \left[\delta + \Delta (v z^2)^{-1/3} + \frac{1}{v} \right] = \Gamma_2 (1 + \delta + \Delta), \quad (\text{C1})$$

where v is defined as $v = u/u_2$, z is defined as $z = r/r_s$, δ is defined as $\delta = 4\pi n_2 \Gamma_2^2 m_p c^2 / B_2^2 \sim u_2/u_1 \sigma$, and Δ is defined as $16\pi P_2 \Gamma_2^2 / B_2^2$. The solution for this equation can be written as

$$v = \frac{1}{2(1 + \Delta)} \frac{G^3}{x^2}, \quad (\text{C2})$$

where

$$G = 1 + \{1 + x^2 + [(1 + x^2)^2 - 1]^{1/2}\}^{1/3} + \{1 + x^2 - [(1 + x^2)^2 - 1]^{1/2}\}^{1/3}, \quad (\text{C3})$$

$$x = z/z_{\Delta}, \tag{C4}$$

and

$$z_{\Delta} = \left[\frac{2}{27} \frac{\Delta^3}{(1 + \Delta)^2} \right]^{1/2}. \tag{C5}$$

Using this solution, we can derive the solution for the total pressure P_T in the postshock in Eq. (22).

REFERENCES

- Ahrens, J., Bai, X., Barouch, G., Barwick, S. W., Bay, R. C., Becka, T., Becker, K.-H., Bertrand, D., Binon, F., et al., 2003, *ApJ*, 583, 1040
- Amato, E., Guetta, D., Blasi, P., 2003 *A&A*, 402, 827
- Atoyan, A. M., Aharonian, F. A., 1996, *MNRAS*, 278, 525, (1996)
- Badhwar, G. D., Stephens, S. A., Golden, R. L., 1977, *Phys. Rev. D*, 15, 820
- Beall, J. H., Bednarek, W., 2002, *ApJ*, 569, 343
- Bednarek, W., Prhoferoe, R. J., 1997, *Phys. Rev. Lett.*, 79, 2616
- Bednarek, W., 2001, *A&A*, 378, 49
- Bednarek, W., Bartosik, M., 2003, *A&A*, 405, 689
- Bednarek, W., 2003, *astro-ph/0305430*
- Bednarek, W., 2003, *astro-ph/0307216*
- Berezinsky, V. S., Gaisser, T. K., Halzen, F., Stanev, T., 1993, *Astropart. Phys.*, 1, 281
- Blasi, P., Epstein, R. I., Olinto, A. V., 2000, *ApJ*, 533, 123
- Blandford, R. D., Ostriker, J. P., 1978, *ApJ*, 221, L29
- Dermer, C. D., 1986a, *ApJ*, 307, 47
- Dermer, C. D., 1986b, *A&A*, 157, 223
- Eichten, E., Hinchliffe, I., Lane, K., Quigg, C., 1984, *Rev. Mod. Phys.*, 56, 579

- Eichten, E., Hinchliffe, I., Lane, K., Quigg, C., 1986, *Rev. Mod. Phys.*, 58, 1065
- Fukuda, Y. et al. (Super-Kamiokande Collaboration) *Phys. Rev. Lett.* **81**, 1562 (1998)
- Gaisser, T. K., Grillo, A. F., 1987, *Phys. Rev. D*, 36, 2752
- Gaisser, T. K., Halzen, F., 1987, *Phys. Rev. Lett.*, 54, 1754
- Granot, J., Guetta, D., 2003, *Phys. Rev. Lett.*, 19, 1102
- Goldreich, P., Julian, W. H., 1969, *ApJ*, 157, 869
- Gould, R. J., 1981, *Phys. Fluids* 24, 102
- Gunn, J. E., Ostriker, J. P., 1969, *Phys. Rev. Lett.*, 22, 728
- Haas, R., Colgan, J., Erickson, F., Lord, D., Burton, G., Hollenbach, J., 1990, *ApJ*, 360, 257
- Hagiwara, K. Hikasa, K., Nakamura, K., Tanabashi, M., Aguilar-Benitez, M., Amsler, C., Barnett, R. M., Burchat, P. R., Carone, C. D., Caso, et al., 2002, *Phys. Rev. D*, 66, 010001
- Hashimoto, M., 1995, *Prog. Theor. Phys.*, 94, 663
- Hester, J. J., Mori, K., Burrows, D., Gallagher, J. S., Graham, J. R., Halverson, M., Kader, A., Michel, F. C., Scowen, P., 2002, *ApJ*, 577, L49
- Honda, M., Kajita, T., Kasahara, K., Midorikawa, S., 1995, *Phys. Rev. D*, 52, 4985
- Hoshino, M., Arons, J., Gallant, Y. A., Langdon, A. B., 1992, *ApJ*, 390, 454
- Kennel C. F., Coroniti, F. V., 1984, *ApJ*, 283, 694
- Landau, L. D., Lifshitz, E. M., 1975, *The Classical Theory of Fields*, 4th Ed., Pergamon, Oxford
- Learned, J. G., Pakvasa, S., 1995, *Astropart. Phys.*, 3, 267
- Mahadevan, R., Narayan, R., Kronik, J., 1997, *ApJ*, 486, 268
- Manchester, R. N., Lyne, A. G., Camilo, F., Kaspi, V. M., Stairs, I. H., Crawford, F., Morris, D., J., Bell, J. F., Amico, N. D., 1999, *astro-ph/9911319*
- Matz, S. M., Share, G. H., Leising, M. D., Chupp, E. L., Vestrand, W. T., Purcell, W. R., Strickman, M. S., Reppin, C., 1988, *Nature*, 331, 416

- Nagataki, S., Hashimoto, M., Sato, K., Yamada, S., 1997, *ApJ*, 486, 1026
- Nagataki, S., 2000, *ApJS*, 127, 141
- Nagataki, S., Kohri, K., Ando, S., Sato, K., 2003, *Astropart. Phys.*, 18, 551
- Nagataki, S., Mizuta, A., Yamada, S., Takabe, H., Sato, K., 2003, *ApJ*, in press.
- Naito, T., Takahara, F., 1994, *J. Phys. G: Nucl. Part. Phys.*, 20, 477
- Reno, M. H., Quigg, C., 1988, *Phys. Rev. D*, 37, 657
- Ruderman, M. A., Sutherland, P. G., 1975, *ApJ*, 196, 51
- Protheroe, R. J., Bednarek, W., Luo, Q., 1998, *Astropart. Phys.*, 9, 1
- Rees, M. J., Gunn, J. E., 1974, *MNRAS*, 167, 1
- Rybicki, G. B., Lightman, A. P., 1979, *Radiative Process in Astrophysics* (New York: John Wiley & Sons)
- Shibata, S., 1991, *ApJ*, 378, 239
- Slane, P., Helfand D. J., Murray, S., 2002, *ApJ*, 571, L45
- Spyromilio, J., Meikle, S., Allen, A., 1990, *MNRAS*, 242, 669
- Stecker, F. W., 1971, *Cosmic Gamma Rays*, NASA SP-249
- Stecker, F. W., 1979, *ApJ*, 228, 919
- Stephens, S. A., Badhwar, G. D., 1981, *Ap&SS*, 76, 213
- Stepney, S., 1983, *MNRAS*, 202, 467
- Thielemann, F.-K., Nomoto, K., Hashimoto, M., 1996, 460, 408
- Torres, D. F., Nuza, S. E., 2003, *ApJ*, 583, L25
- Waxman, E., Bahcall, J. N., 1997, *Phys. Rev. Lett.*, 78, 2292
- Woosley, S. E., Weaver, T. A., 1995, *ApJS*, 101, 181

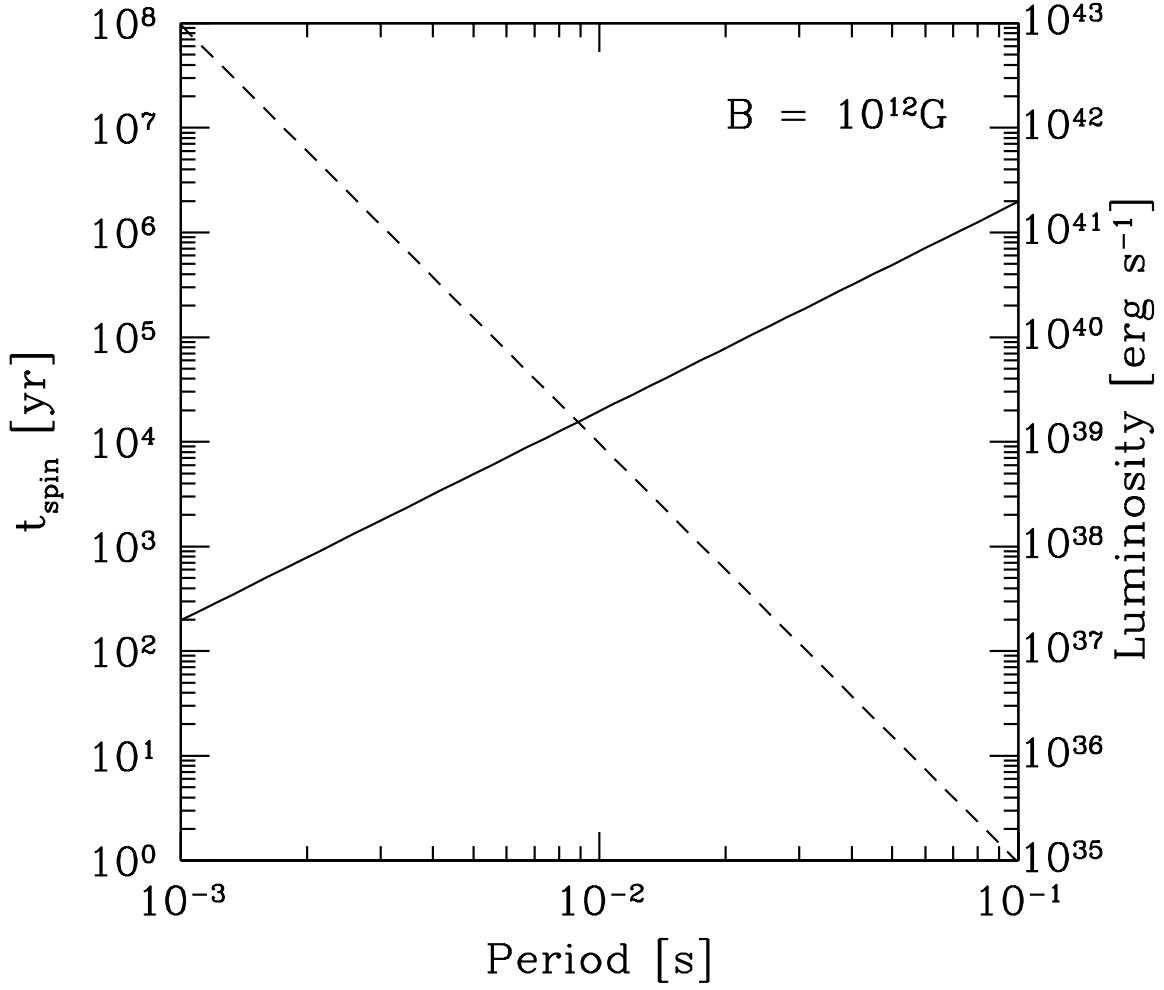


Fig. 1.— Solid line: spin down age [yr] as a function of period of a pulsar. Spin down age is defined as the time interval for a pulsar’s angular velocity to become half of the initial one. Dashed line: spin down luminosity as a function of a period of a pulsar. In this study, wind luminosity is assumed to be comparable with the spin down luminosity. Amplitude of the magnetic field at the pole of a pulsar is set to be 10^{12}G throughout in this study.

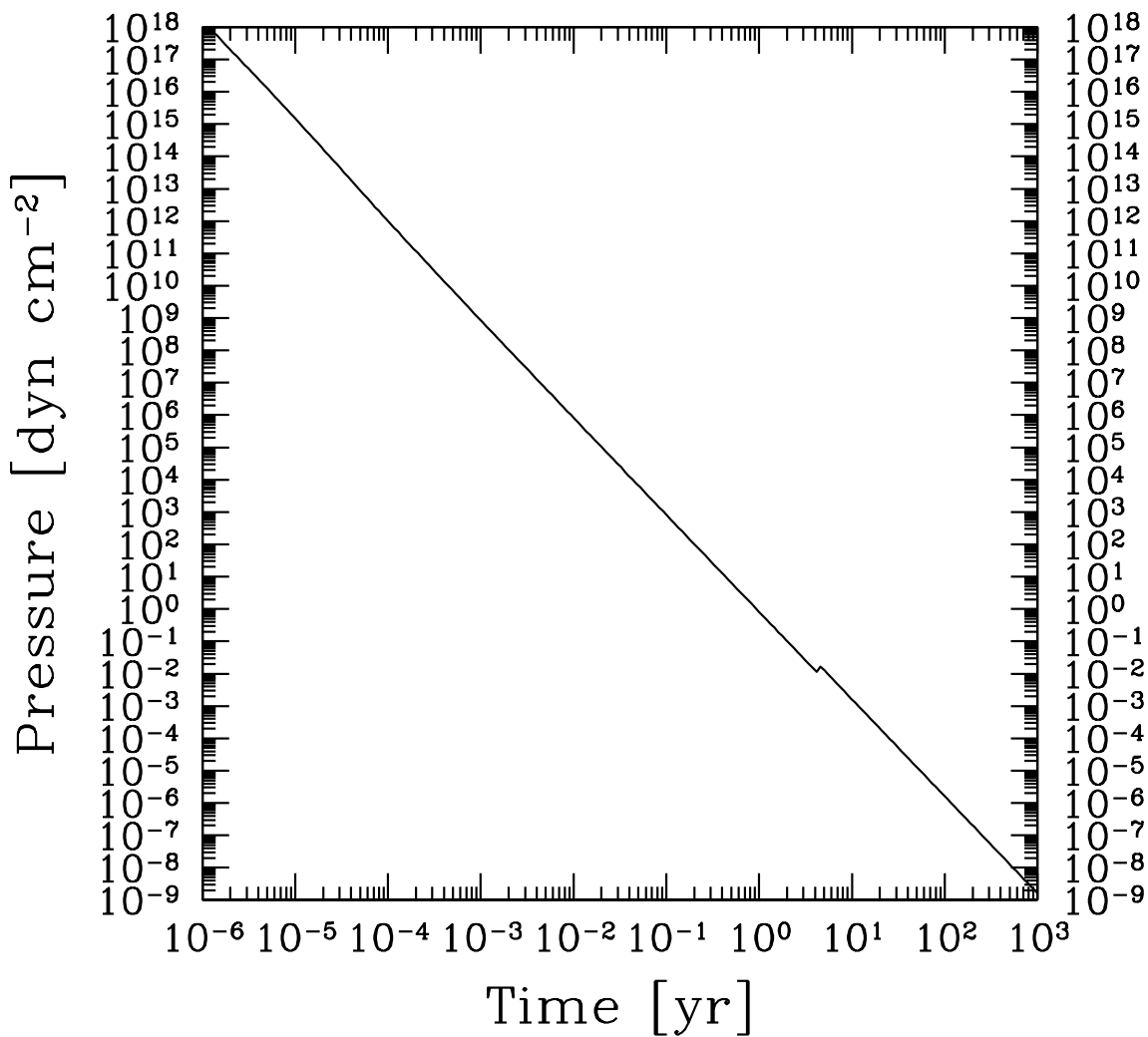


Fig. 2.— Relation between pressure [dyn cm⁻²] and age [yr] of the innermost region of the remnant. The discontinuity at $t \sim 5$ yr reflects the transition from photon-dominated phase to matter-dominated phase. This happens when the optical depth of the supernova ejecta becomes lower than unity and pressure of photon fields is set to be zero.

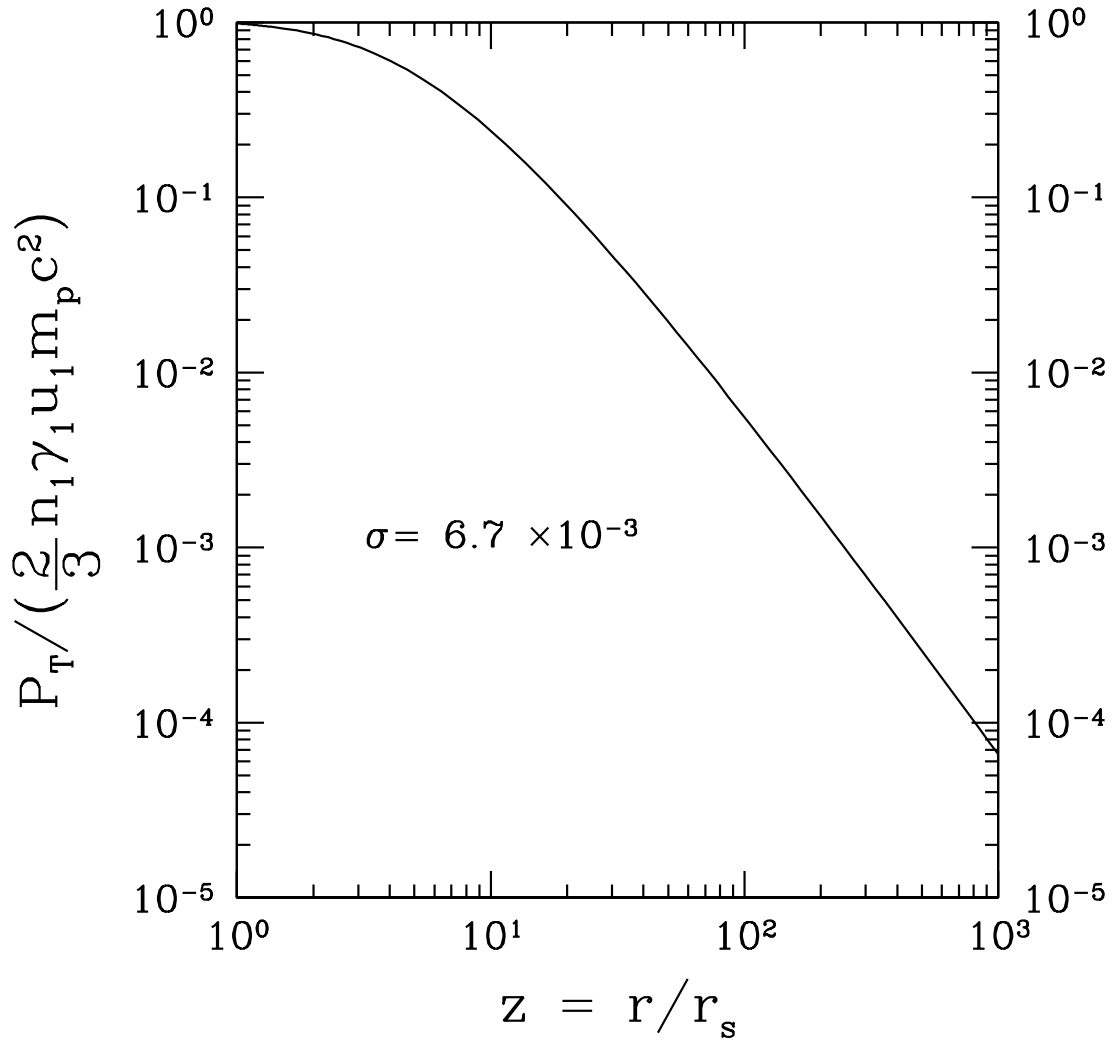


Fig. 3.— Total pressure as a function of $z = r/r_s$, normalized by $2n_1\gamma_1u_1m_p c^2/3$. σ is set to be $6.7 \times 10^{-3} \equiv \sigma_c$.

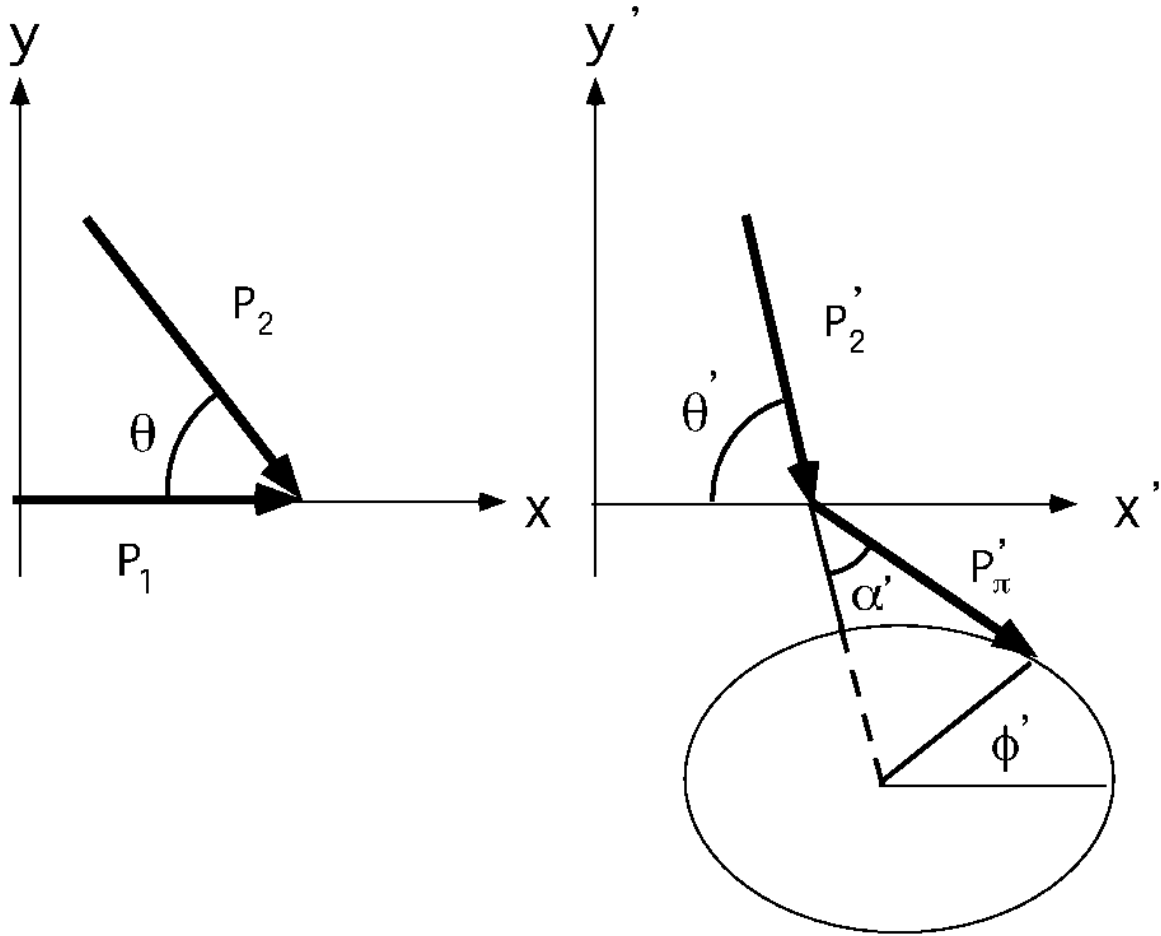


Fig. 4.— Sketch of the geometry concerning the individual scattering events. The left panel shows the geometry in the fluid-rest frame, while the right panel shows the geometry in the rest frame of particle 1.

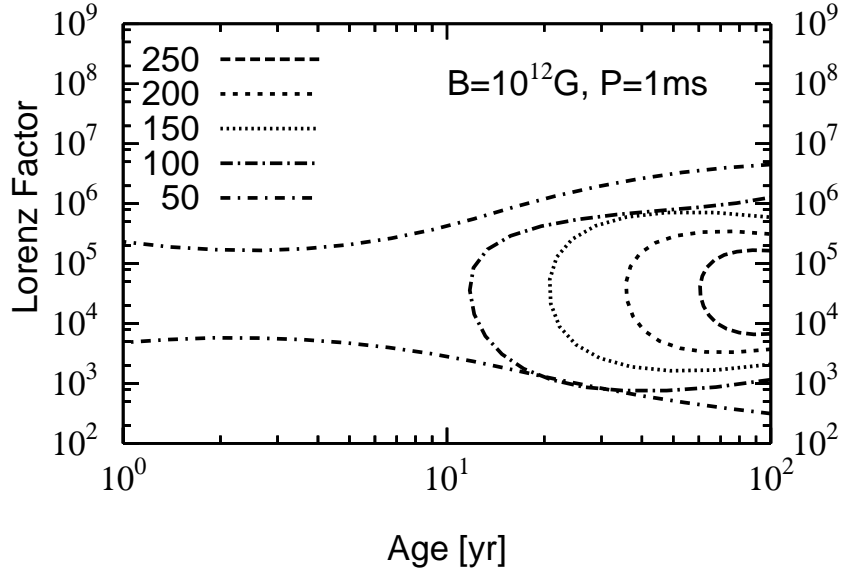


Fig. 5.— Contour of the neutrino event whose energy is greater than 10 GeV per year for a km^3 detector of high-energy neutrinos as functions of age [yr] of a pulsar and initial bulk Lorentz factor of the pulsar wind. The pulsar is assumed to be located 10 kpc away from the earth. The amplitude of the magnetic field and period of the pulsar are assumed to be 10^{12} G and 1ms. It is noted that the spin down age is about 2×10^2 yr, so that the range of the age is limited to be within 10^2 yr. Also, when the age of the pulsar is about 10^{-1} yr, synchrotron cooling timescale and/or energy transfer timescale from protons to electrons are so short that the Maxwellian distribution of protons is distorted and production of pions is severely limited (see table 2). As for the bulk Lorentz factor of the initial pulsar wind, the maximum value is determined by Eq.(28). When the bulk Lorentz factor is about 10^1 , the energy transfer timescale from protons to electrons are too short (see table 2).

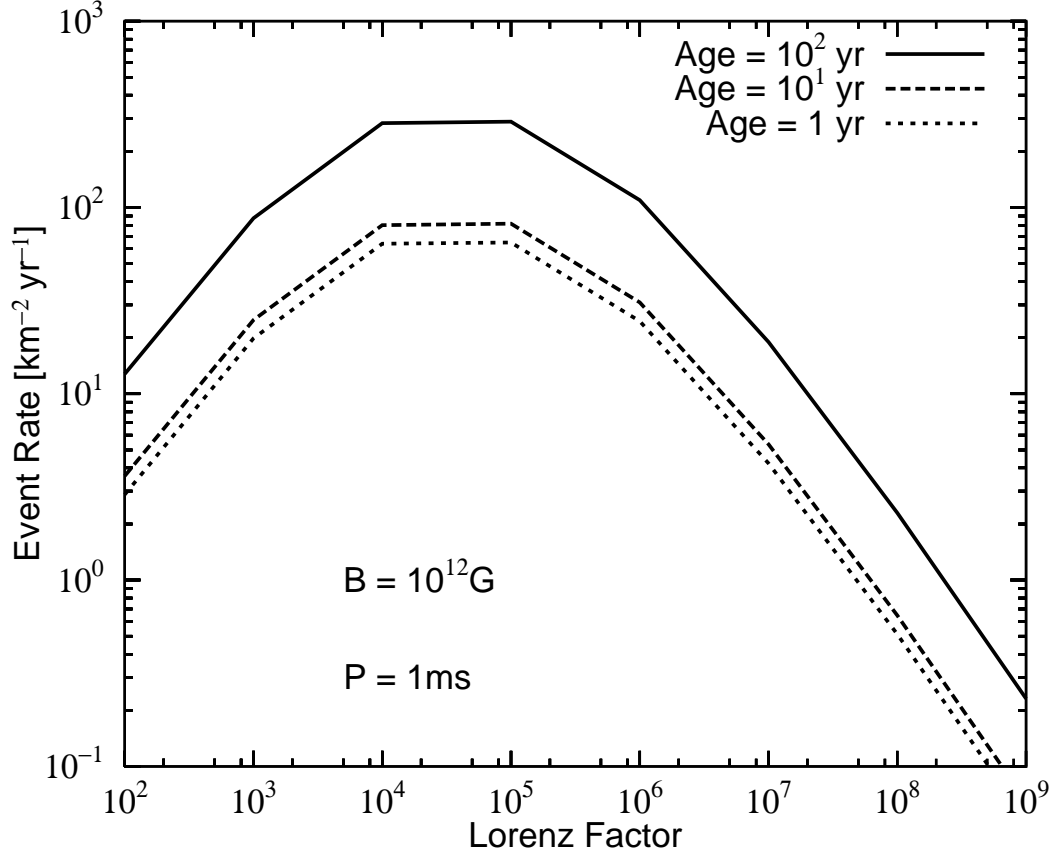


Fig. 6.— Same with figure 5, but horizontal line represents the initial bulk Lorentz factor of pulsar wind with the age of the pulsar fixed as 1 (Models C2-C9), 10^1 (Models B2-B9), and 10^2 yr (Models A2-A9). The reason for the event rate to become smaller for the case of large initial Lorentz factor is that the number density of protons behind the termination shock wave becomes smaller (see figure 7). Also, the reason for the event rate to become smaller for the case of the Lorentz factor to be smaller than 10^4 is that high energy protons do not exist and high energy neutrinos are not produced. It is noted that the cross section between neutrino and quark is roughly proportional to energy of neutrinos in the quark-rest frame.

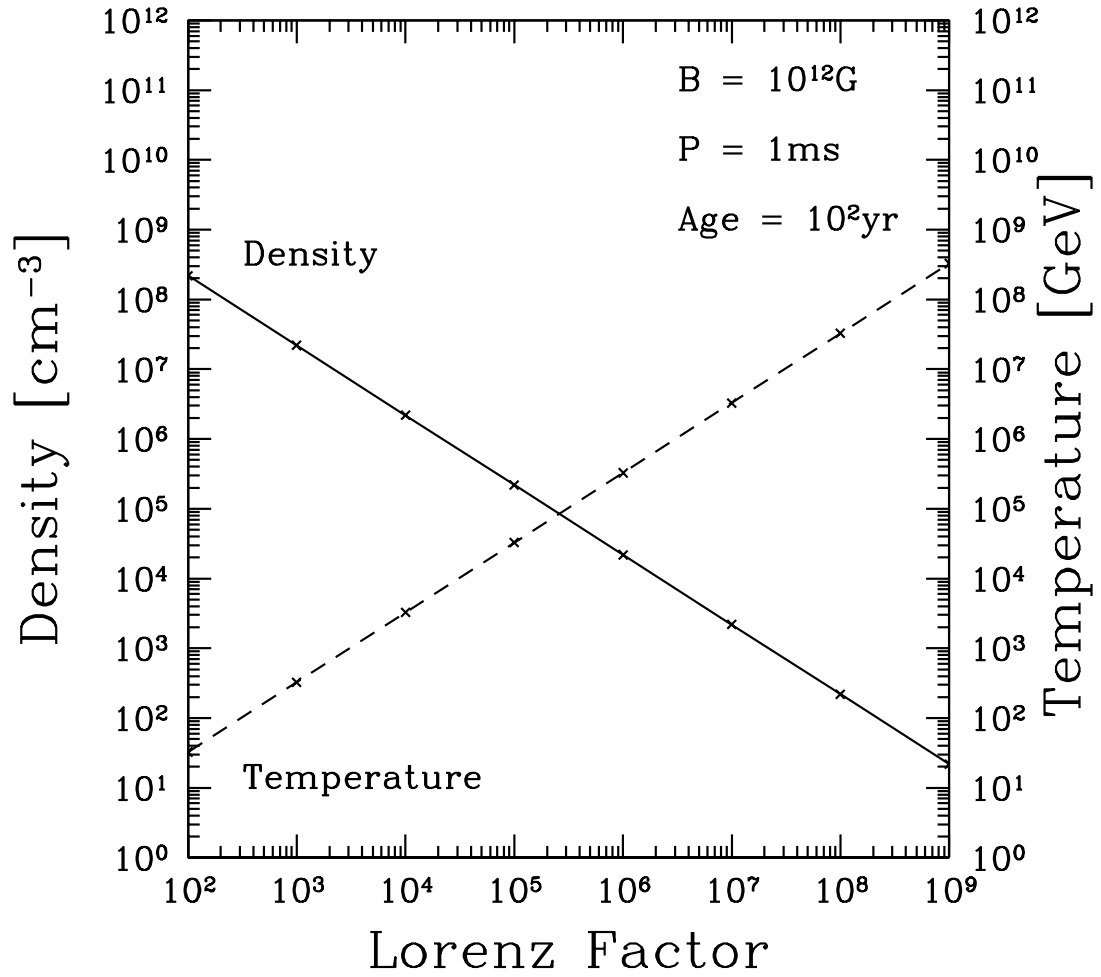


Fig. 7.— The density (solid line) and temperature (dashed line) behind the termination shock wave as a function of the initial bulk Lorentz factor of the pulsar wind. The amplitude of the magnetic field, period, and age of the pulsar are assumed to be 10^{12} G , 1 ms , and 10^2 yr (Models A2-A9).

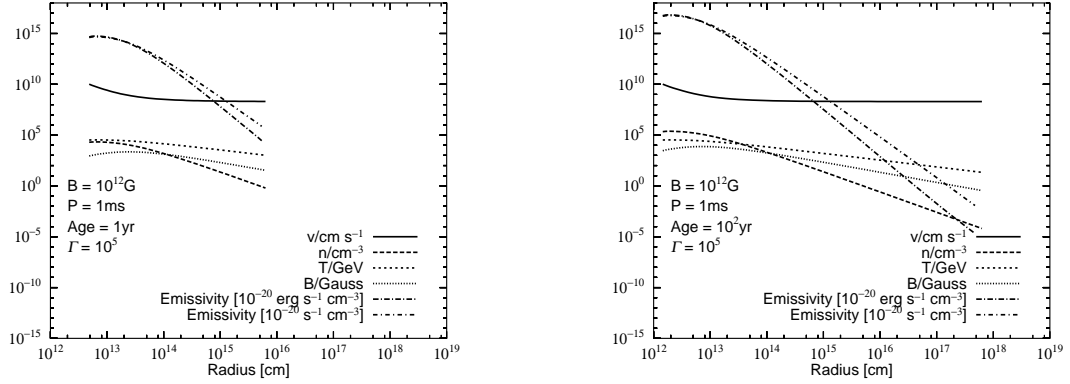


Fig. 8.— Profiles of velocity, number density of protons, temperature, magnetic field, and emissivity of charged pions in units of $[10^{-20}\text{erg s}^{-1} \text{cm}^{-3}]$ and $[10^{-20}\text{particles s}^{-1} \text{cm}^{-3}]$. The inner and outer boundaries correspond to the location of the termination shock wave and the innermost region of the surrounding supernova remnant. The amplitude of the magnetic field and period of the pulsar are assumed to be 10^{12}G and 1ms . Initial bulk Lorentz factor of the pulsar wind is set to be 10^5 . The left panel represents the case that the age of the pulsar is 1 yr (Models C5), while the right panel shows the case that the age of the pulsar is 10^2 yr (Models A5).

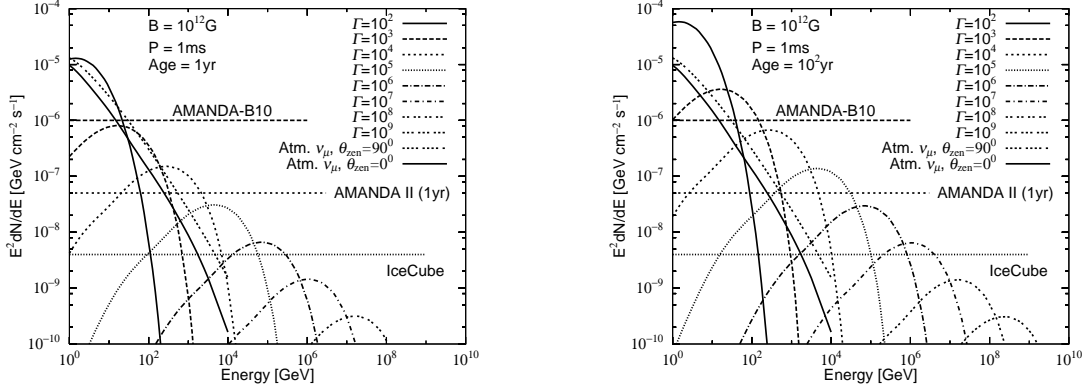


Fig. 9.— Spectrum of energy fluxes of neutrinos from a pulsar which is located 10 kpc away from the earth. The amplitude of the magnetic field and period of the pulsar is assumed to be 10^{12}G and 1ms . The minimum detectable energy flux of AMANDA-B10, AMANDA II (1yr), and IceCube is represented by horizontal lines. The atmospheric neutrino energy fluxes for a circular patch of 1° are also shown. The left panel represents the case that the age of the pulsar is 1 yr (Models C2-C9), while right panel represent the case that the age is 10^2yr (Models A2-A9).

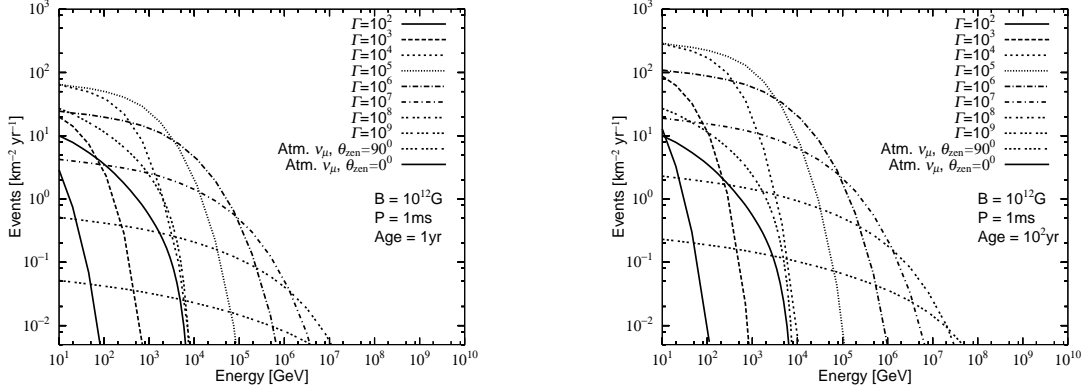


Fig. 10.— Neutrino event rate per year from a pulsar wind as a function of the muon energy threshold in a km^3 high-energy neutrino detector. The pulsar is assumed to be located 10 kpc away from the earth. The amplitude of the magnetic field and period of the pulsar is assumed to be 10^{12}G and 1ms. The left panel represents the case that the age of the pulsar is 1yr (Models C2-C9), while right panel represents the case that the age is 10^2yr (Models A2-A9). The event rates expected of atmospheric neutrino for a circular patch of 1° are also shown. The event rates are shown for the vertical downgoing atmospheric neutrinos and horizontal ones.

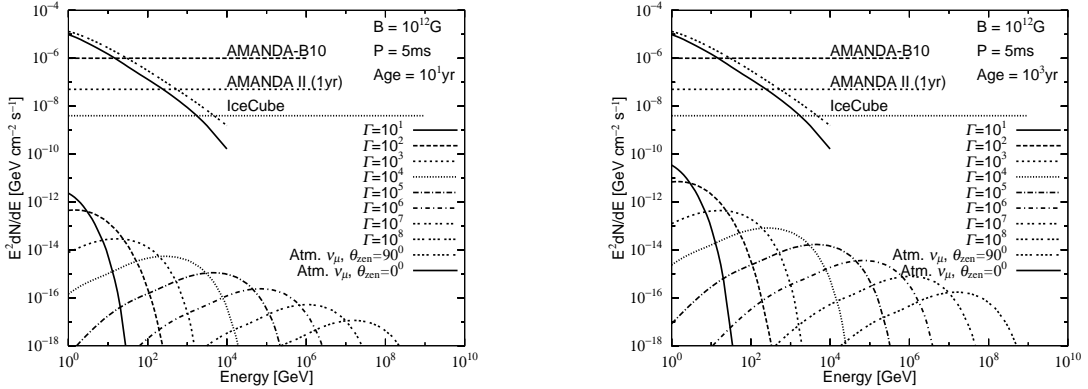


Fig. 11.— Same as figure 9, but for the period of the pulsar is 5ms. The left panel represents the case that the age of the pulsar is 10yr (Models G1-G8), while right panel represent the case that the age is 10^3yr (Models E1-E8). Note that the scale of the vertical line is different from that of figure 9.

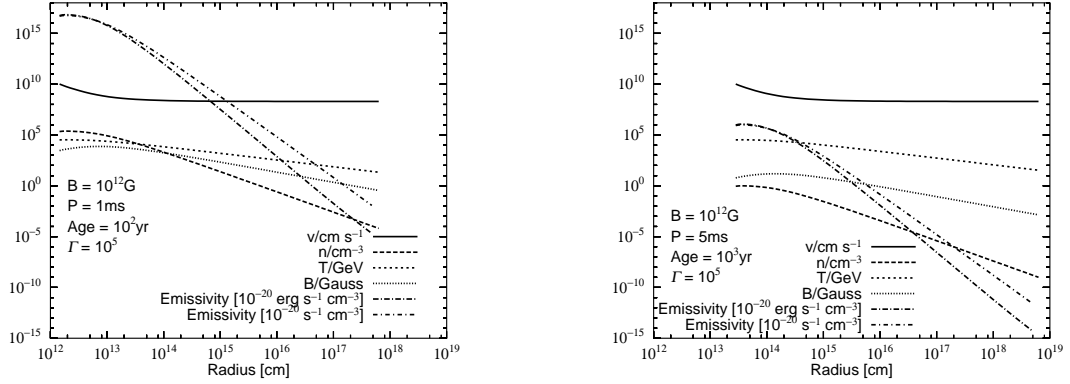


Fig. 12.— Profiles of velocity, number density of protons, temperature, magnetic field, and emissivity of charged pions in units of $[10^{-20}\text{erg s}^{-1}\text{cm}^{-3}]$ and $[10^{-20}\text{particles s}^{-1}\text{cm}^{-3}]$. The inner and outer boundaries correspond to the location of the termination shock wave and the innermost region of the surrounding supernova remnant. The amplitude of the magnetic field is assumed to be 10^{12}G . Initial bulk Lorentz factor of the pulsar wind is set to be 10^5 . The left panel represents the case that the period and age of the pulsar are 1ms and 10^2 yr (Model A5; same with the right panel of figure 8), while the right panel shows the case that the period and age of the pulsar are 5ms and 10^3 yr (Model E5).

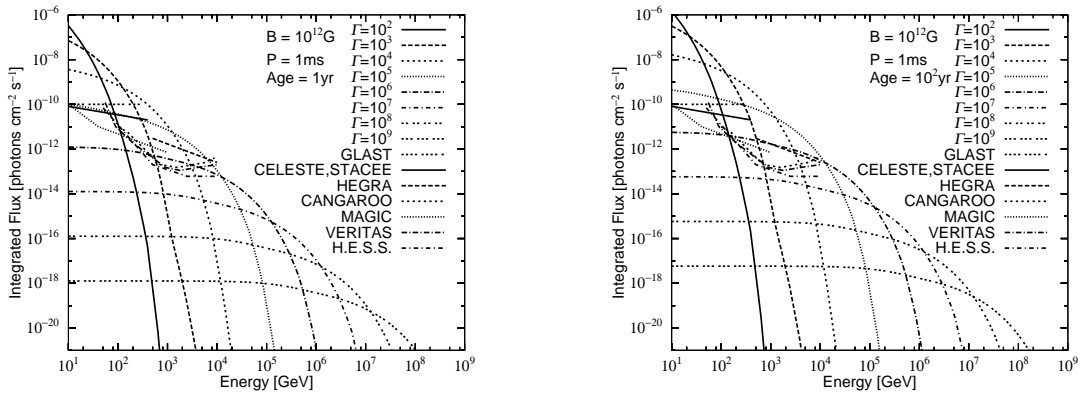


Fig. 13.— Integrated gamma-ray fluxes from the neutral pion decays are shown. The amplitude of the magnetic field and period of the pulsar are assumed to be 10^{12}G and 1ms. The left panel represents the case that the age of the pulsar is 1yr (Models C2-C9), while the right panel shows the case that the age of the pulsar is 10^2 yr (Models A2-A9). The minimum detectable integrated fluxes of GLAST, STACEE, CELESTE, HEGRA, CANGAROO, MAGIC, VERITAS, and H.E.S.S. are also shown.

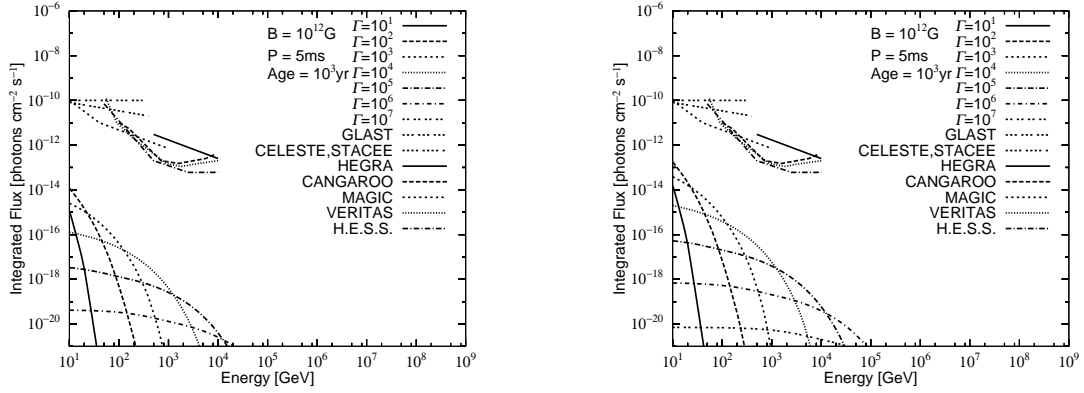


Fig. 14.— Same with figure 13, but for the case that the period of the pulsar is 5ms. The left panel represents the case that the age of the pulsar is 10yr (Models G1-G8), while the right panel shows the case that the age of the pulsar is 10^3 yr (Models E1-E8).

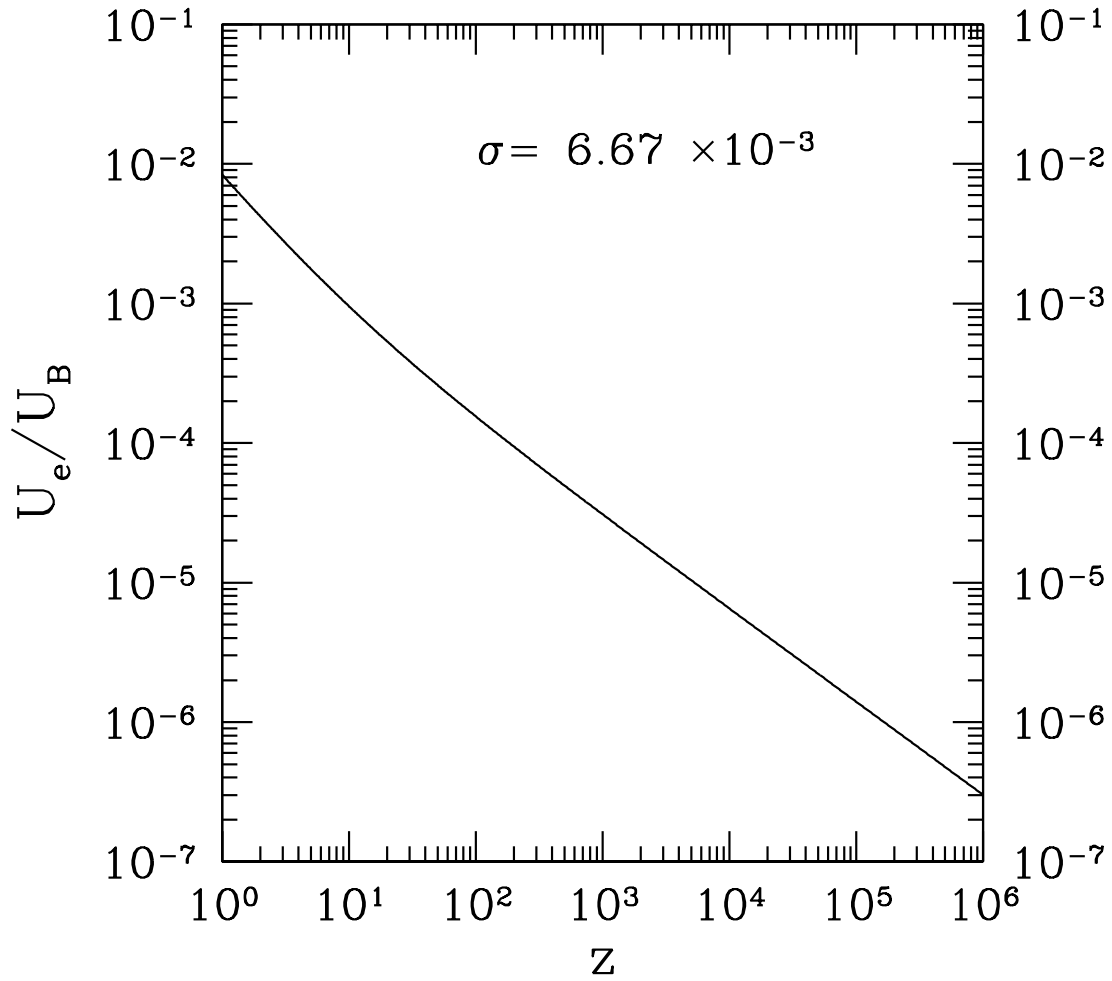


Fig. 15.— Ratio of the thermal energy of electrons relative to the energy of electric-magnetic fields as a function of z ($\equiv r/r_s$) in the case where $n_e = n_p$. Definition of σ is shown in Eq.(1) and set to be $\sigma_c = 6.67 \times 10^{-3}$.

Table 1. Parameters for the representation of invariant cross section

Particle	A [mb/(GeV ² /c ³)]	B [(GeV/c) ⁻¹]	r	C_1	C_2 [(GeV/c) ⁻¹]	C_3 [(GeV/c) ⁻²]
π^0	140	5.43	2	6.1	-3.3	0.6
π^+	153	5.55	1	5.37	-3.5	0.83
π^-	127	5.30	3	7.03	-4.5	1.67

Table 2. Input and Output Parameters

Model	B [G]	P [ms]	L [erg s ⁻¹]	Age [yr]	Γ	r_{shock} [cm]	$t_{\text{min}}^{\text{a}}$	$\min(t_{\text{min}}, t_{\text{ep}})^{\text{b}}$	L_{π} [erg s ⁻¹]	Event Rate [km ⁻² yr ⁻¹]
Model A1	10 ¹²	1	9.6 × 10 ⁴²	10 ²	10 ¹	1.5 × 10 ¹²	t_{travel}	t_{ep}	—	—
Model A2	10 ¹²	1	9.6 × 10 ⁴²	10 ²	10 ²	1.5 × 10 ¹²	t_{travel}	t_{travel}	5.5 × 10 ³⁹	1.3 × 10 ¹
Model A3	10 ¹²	1	9.6 × 10 ⁴²	10 ²	10 ³	1.5 × 10 ¹²	t_{travel}	t_{travel}	2.6 × 10 ³⁸	8.8 × 10 ¹
Model A4	10 ¹²	1	9.6 × 10 ⁴²	10 ²	10 ⁴	1.5 × 10 ¹²	t_{travel}	t_{travel}	2.6 × 10 ³⁷	2.8 × 10 ²
Model A5	10 ¹²	1	9.6 × 10 ⁴²	10 ²	10 ⁵	1.5 × 10 ¹²	t_{travel}	t_{travel}	2.7 × 10 ³⁶	2.9 × 10 ²
Model A6	10 ¹²	1	9.6 × 10 ⁴²	10 ²	10 ⁶	1.5 × 10 ¹²	t_{travel}	t_{travel}	2.7 × 10 ³⁵	1.1 × 10 ²
Model A7	10 ¹²	1	9.6 × 10 ⁴²	10 ²	10 ⁷	1.5 × 10 ¹²	t_{travel}	t_{travel}	2.7 × 10 ³⁴	1.9 × 10 ¹
Model A8	10 ¹²	1	9.6 × 10 ⁴²	10 ²	10 ⁸	1.5 × 10 ¹²	t_{travel}	t_{travel}	2.7 × 10 ³³	2.3 × 10 ⁰
Model A9	10 ¹²	1	9.6 × 10 ⁴²	10 ²	10 ⁹	1.5 × 10 ¹²	t_{travel}	t_{travel}	2.7 × 10 ³²	2.3 × 10 ⁻¹
Model B1	10 ¹²	1	9.6 × 10 ⁴²	10 ¹	10 ¹	4.3 × 10 ¹²	t_{travel}	t_{ep}	—	—
Model B2	10 ¹²	1	9.6 × 10 ⁴²	10 ¹	10 ²	4.3 × 10 ¹²	t_{travel}	t_{travel}	1.5 × 10 ³⁹	3.6 × 10 ⁰
Model B3	10 ¹²	1	9.6 × 10 ⁴²	10 ¹	10 ³	4.3 × 10 ¹²	t_{travel}	t_{travel}	7.5 × 10 ³⁷	2.5 × 10 ¹
Model B4	10 ¹²	1	9.6 × 10 ⁴²	10 ¹	10 ⁴	4.3 × 10 ¹²	t_{travel}	t_{travel}	7.5 × 10 ³⁶	8.0 × 10 ¹
Model B5	10 ¹²	1	9.6 × 10 ⁴²	10 ¹	10 ⁵	4.3 × 10 ¹²	t_{travel}	t_{travel}	7.6 × 10 ³⁵	8.2 × 10 ¹
Model B6	10 ¹²	1	9.6 × 10 ⁴²	10 ¹	10 ⁶	4.3 × 10 ¹²	t_{travel}	t_{travel}	7.6 × 10 ³⁴	3.1 × 10 ¹
Model B7	10 ¹²	1	9.6 × 10 ⁴²	10 ¹	10 ⁷	4.3 × 10 ¹²	t_{travel}	t_{travel}	7.6 × 10 ³³	5.3 × 10 ⁰
Model B8	10 ¹²	1	9.6 × 10 ⁴²	10 ¹	10 ⁸	4.3 × 10 ¹²	t_{travel}	t_{travel}	7.6 × 10 ³²	6.5 × 10 ⁻¹
Model B9	10 ¹²	1	9.6 × 10 ⁴²	10 ¹	10 ⁹	4.3 × 10 ¹²	t_{travel}	t_{travel}	7.6 × 10 ³¹	6.5 × 10 ⁻²
Model C1	10 ¹²	1	9.6 × 10 ⁴²	10 ⁰	10 ¹	4.8 × 10 ¹²	t_{travel}	t_{ep}	—	—
Model C2	10 ¹²	1	9.6 × 10 ⁴²	10 ⁰	10 ²	4.8 × 10 ¹²	t_{travel}	t_{travel}	5.9 × 10 ³⁸	2.9 × 10 ⁰
Model C3	10 ¹²	1	9.6 × 10 ⁴²	10 ⁰	10 ³	4.8 × 10 ¹²	t_{travel}	t_{travel}	5.9 × 10 ³⁷	2.0 × 10 ¹
Model C4	10 ¹²	1	9.6 × 10 ⁴²	10 ⁰	10 ⁴	4.8 × 10 ¹²	t_{travel}	t_{travel}	5.9 × 10 ³⁶	6.4 × 10 ¹
Model C5	10 ¹²	1	9.6 × 10 ⁴²	10 ⁰	10 ⁵	4.8 × 10 ¹²	t_{travel}	t_{travel}	6.0 × 10 ³⁵	6.5 × 10 ¹
Model C6	10 ¹²	1	9.6 × 10 ⁴²	10 ⁰	10 ⁶	4.8 × 10 ¹²	t_{travel}	t_{travel}	6.0 × 10 ³⁴	2.4 × 10 ¹
Model C7	10 ¹²	1	9.6 × 10 ⁴²	10 ⁰	10 ⁷	4.8 × 10 ¹²	t_{travel}	t_{travel}	6.0 × 10 ³³	4.2 × 10 ⁰
Model C8	10 ¹²	1	9.6 × 10 ⁴²	10 ⁰	10 ⁸	4.8 × 10 ¹²	t_{travel}	t_{travel}	6.0 × 10 ³²	5.1 × 10 ⁻¹
Model C9	10 ¹²	1	9.6 × 10 ⁴²	10 ⁰	10 ⁹	4.8 × 10 ¹²	t_{travel}	t_{travel}	6.0 × 10 ³¹	5.1 × 10 ⁻²
Model D1	10 ¹²	1	9.6 × 10 ⁴²	10 ⁻¹	10 ¹	1.0 × 10 ⁶	t_{col}	t_{ep}	—	—
Model D2	10 ¹²	1	9.6 × 10 ⁴²	10 ⁻¹	10 ²	1.0 × 10 ⁶	t_{col}	t_{ep}	—	—
Model D3	10 ¹²	1	9.6 × 10 ⁴²	10 ⁻¹	10 ³	1.0 × 10 ⁶	t_{col}	t_{col}	—	—
Model D4	10 ¹²	1	9.6 × 10 ⁴²	10 ⁻¹	10 ⁴	1.0 × 10 ⁶	t_{sync}	t_{sync}	—	—
Model D5	10 ¹²	1	9.6 × 10 ⁴²	10 ⁻¹	10 ⁵	1.0 × 10 ⁶	t_{sync}	t_{sync}	—	—
Model D6	10 ¹²	1	9.6 × 10 ⁴²	10 ⁻¹	10 ⁶	1.0 × 10 ⁶	t_{sync}	t_{sync}	—	—
Model D7	10 ¹²	1	9.6 × 10 ⁴²	10 ⁻¹	10 ⁷	1.0 × 10 ⁶	t_{sync}	t_{sync}	—	—
Model D8	10 ¹²	1	9.6 × 10 ⁴²	10 ⁻¹	10 ⁸	1.0 × 10 ⁶	t_{sync}	t_{sync}	—	—
Model D9	10 ¹²	1	9.6 × 10 ⁴²	10 ⁻¹	10 ⁹	1.0 × 10 ⁶	t_{sync}	t_{sync}	—	—
Model E1	10 ¹⁵	5	1.5 × 10 ⁴⁰	10 ³	10 ¹	2.8 × 10 ¹³	t_{travel}	t_{travel}	5.1 × 10 ³³	3.0 × 10 ⁻⁹
Model E2	10 ¹⁵	5	1.5 × 10 ⁴⁰	10 ³	10 ²	2.8 × 10 ¹³	t_{travel}	t_{travel}	6.7 × 10 ³²	1.6 × 10 ⁻⁶
Model E3	10 ¹⁵	5	1.5 × 10 ⁴⁰	10 ³	10 ³	2.8 × 10 ¹³	t_{travel}	t_{travel}	3.2 × 10 ³¹	1.1 × 10 ⁻⁵
Model E4	10 ¹⁵	5	1.5 × 10 ⁴⁰	10 ³	10 ⁴	2.8 × 10 ¹³	t_{travel}	t_{travel}	3.2 × 10 ³⁰	3.5 × 10 ⁻⁵
Model E5	10 ¹⁵	5	1.5 × 10 ⁴⁰	10 ³	10 ⁵	2.8 × 10 ¹³	t_{travel}	t_{travel}	3.3 × 10 ²⁹	3.5 × 10 ⁻⁵
Model E6	10 ¹⁵	5	1.5 × 10 ⁴⁰	10 ³	10 ⁶	2.8 × 10 ¹³	t_{travel}	t_{travel}	3.3 × 10 ²⁸	1.3 × 10 ⁻⁵
Model E7	10 ¹⁵	5	1.5 × 10 ⁴⁰	10 ³	10 ⁷	2.8 × 10 ¹³	t_{travel}	t_{travel}	3.3 × 10 ²⁷	2.3 × 10 ⁻⁶
Model E8	10 ¹⁵	5	1.5 × 10 ⁴⁰	10 ³	10 ⁸	2.8 × 10 ¹³	t_{travel}	t_{travel}	3.3 × 10 ²⁶	2.8 × 10 ⁻⁷
Model F1	10 ¹²	5	1.5 × 10 ⁴⁰	10 ²	10 ¹	8.9 × 10 ¹³	t_{travel}	t_{travel}	1.4 × 10 ³³	8.3 × 10 ⁻¹⁰
Model F2	10 ¹²	5	1.5 × 10 ⁴⁰	10 ²	10 ²	8.9 × 10 ¹³	t_{travel}	t_{travel}	1.8 × 10 ³²	4.2 × 10 ⁻⁷
Model F3	10 ¹²	5	1.5 × 10 ⁴⁰	10 ²	10 ³	8.9 × 10 ¹³	t_{travel}	t_{travel}	8.7 × 10 ³⁰	2.9 × 10 ⁻⁶
Model F4	10 ¹²	5	t_{travel}	10 ²	10 ⁴	8.9 × 10 ¹³	t_{travel}	t_{travel}	8.8 × 10 ²⁹	9.4 × 10 ⁻⁶

Table 2—Continued

Model	B [G]	P [ms]	L [erg s ⁻¹]	Age [yr]	Γ	r_{shock} [cm]	$t_{\text{min}}^{\text{a}}$	$\min(t_{\text{min}}, t_{\text{ep}})^{\text{b}}$	L_{π} [erg s ⁻¹]	Event Rate [km ⁻² yr ⁻¹]
Model F5	10 ¹²	5	1.5 × 10 ⁴⁰	10 ²	10 ⁵	8.9 × 10 ¹³	t_{travel}	t_{travel}	8.8 × 10 ²⁸	9.5 × 10 ⁻⁶
Model F6	10 ¹²	5	1.5 × 10 ⁴⁰	10 ²	10 ⁶	8.9 × 10 ¹³	t_{travel}	t_{travel}	8.8 × 10 ²⁷	3.6 × 10 ⁻⁶
Model F7	10 ¹²	5	1.5 × 10 ⁴⁰	10 ²	10 ⁷	8.9 × 10 ¹³	t_{travel}	t_{travel}	8.8 × 10 ²⁶	6.2 × 10 ⁻⁷
Model F8	10 ¹²	5	1.5 × 10 ⁴⁰	10 ²	10 ⁸	8.9 × 10 ¹³	t_{travel}	t_{travel}	8.8 × 10 ²⁵	7.6 × 10 ⁻⁸
Model G1	10 ¹²	5	1.5 × 10 ⁴⁰	10 ¹	10 ¹	8.9 × 10 ¹³	t_{travel}	t_{travel}	3.4 × 10 ³²	2.1 × 10 ⁻¹⁰
Model G2	10 ¹²	5	1.5 × 10 ⁴⁰	10 ¹	10 ²	3.0 × 10 ¹⁴	t_{travel}	t_{travel}	4.3 × 10 ³¹	1.0 × 10 ⁻⁷
Model G3	10 ¹²	5	1.5 × 10 ⁴⁰	10 ¹	10 ³	3.0 × 10 ¹⁴	t_{travel}	t_{travel}	2.1 × 10 ³⁰	7.2 × 10 ⁻⁷
Model G4	10 ¹²	5	1.5 × 10 ⁴⁰	10 ¹	10 ⁴	3.0 × 10 ¹⁴	t_{travel}	t_{travel}	2.1 × 10 ²⁹	2.3 × 10 ⁻⁶
Model G5	10 ¹²	5	1.5 × 10 ⁴⁰	10 ¹	10 ⁵	3.0 × 10 ¹⁴	t_{travel}	t_{travel}	2.1 × 10 ²⁸	2.3 × 10 ⁻⁶
Model G6	10 ¹²	5	1.5 × 10 ⁴⁰	10 ¹	10 ⁶	3.0 × 10 ¹⁴	t_{travel}	t_{travel}	2.1 × 10 ²⁷	8.8 × 10 ⁻⁷
Model G7	10 ¹²	5	1.5 × 10 ⁴⁰	10 ¹	10 ⁷	3.0 × 10 ¹⁴	t_{travel}	t_{travel}	2.1 × 10 ²⁶	1.5 × 10 ⁻⁷
Model G8	10 ¹²	5	1.5 × 10 ⁴⁰	10 ¹	10 ⁸	3.0 × 10 ¹⁴	t_{travel}	t_{travel}	2.1 × 10 ²⁵	1.8 × 10 ⁻⁸
Model H1	10 ¹²	5	1.5 × 10 ⁴⁰	10 ⁰	10 ¹	1.0 × 10 ⁶	t_{travel}	t_{ep}	—————	—————
Model H2	10 ¹²	5	1.5 × 10 ⁴⁰	10 ⁰	10 ²	1.0 × 10 ⁶	t_{travel}	t_{ep}	—————	—————
Model H3	10 ¹²	5	1.5 × 10 ⁴⁰	10 ⁰	10 ³	1.0 × 10 ⁶	t_{travel}	t_{travel}	1.5 × 10 ³⁹	4.9 × 10 ²
Model H4	10 ¹²	5	1.5 × 10 ⁴⁰	10 ⁰	10 ⁴	1.0 × 10 ⁶	t_{travel}	t_{travel}	1.5 × 10 ³⁸	1.6 × 10 ³
Model H5	10 ¹²	5	1.5 × 10 ⁴⁰	10 ⁰	10 ⁵	1.0 × 10 ⁶	t_{sync}	t_{sync}	—————	—————
Model H6	10 ¹²	5	1.5 × 10 ⁴⁰	10 ⁰	10 ⁶	1.0 × 10 ⁶	t_{sync}	t_{sync}	—————	—————
Model H7	10 ¹²	5	1.5 × 10 ⁴⁰	10 ⁰	10 ⁷	1.0 × 10 ⁶	t_{sync}	t_{sync}	—————	—————
Model H8	10 ¹²	5	1.5 × 10 ⁴⁰	10 ⁰	10 ⁸	1.0 × 10 ⁶	t_{sync}	t_{sync}	—————	—————

^a Shortest timescale among proton’s synchrotron cooling timescale t_{sync} , traveling timescale t_{travel} , and collision timescale t_{col} . When $t_{\text{min}} = t_{\text{travel}}$ or t_{col} , it means that t_{min} is always shorter than t_{sync} . On the other hand, when $t_{\text{min}} = t_{\text{col}}$, it means that t_{col} is shorter than any other timescales at some region of the nebula flow.

^b Shorter timescale between t_{min} and energy transfer timescale from protons to electrons t_{ep} . When $\min(t_{\text{min}}, t_{\text{ep}}) = t_{\text{min}}$, it means that t_{min} is always shorter than t_{ep} in the nebula flow. On the other hand, when $\min(t_{\text{min}}, t_{\text{ep}}) = t_{\text{ep}}$, it means that t_{ep} is shorter than t_{min} at some region of the nebula flow.

Note. — Luminosity of pions (L_{π}) and event rate at a km³ high-energy neutrino detector are not shown when the conditions (i)-(iii) presented in section 3 are not satisfied.